

Histone H1 deamidation facilitates chromatin relaxation for DNA repair

<https://doi.org/10.1038/s41586-025-08835-0>

Received: 18 December 2023

Accepted: 24 February 2025

Published online: 16 April 2025

Open access

 Check for updates

Yuan Tian^{1,6}, Tingting Feng^{1,6}, Jun Zhang^{1,6}, Qingren Meng¹, Wenxin Zhan¹, Ming Tang², Chaohua Liu³, Mengyan Li¹, Wenhui Tao¹, Yuxin Shu⁴, Yu Zhang^{1,5}, Feng Chen¹, Shunichi Takeda¹, Qian Zhu¹, Xiaopeng Lu¹ & Wei-Guo Zhu^{1,4✉}

The formation of accessible chromatin around DNA double-strand breaks is essential for their efficient repair¹. Although the linker histone H1 is known to facilitate higher-order chromatin compaction^{2,3}, the mechanisms by which H1 modifications regulate chromatin relaxation in response to DNA damage are unclear. Here we show that CTP synthase 1 (CTPS1)-catalysed deamidation of H1 asparagine residues 76 and 77 triggers the sequential acetylation of lysine 75 following DNA damage, and this dual modification of H1 is associated with chromatin opening. Mechanistically, the histone acetyltransferase p300 showed a preference for deamidated H1 as a substrate, establishing H1 deamidation as a prerequisite for subsequent acetylation. Moreover, high expression of CTPS1 was associated with resistance to cancer radiotherapy, in both mouse xenograft models and clinical cohorts. These findings provide new insights into how linker histones regulate dynamic chromatin alterations in the DNA damage response.

Double-strand breaks (DSBs) are among the most severe forms of DNA damage, as they induce genomic instability. Their efficient repair requires increased chromatin accessibility to facilitate the recruitment of repair factors¹. The most well-characterized mechanisms for the rapid opening of chromatin involve acetylation and protein poly(ADP-ribosylation) (PARylation), which reduce the charge at the DNA–nucleosome interface^{4–10}. The mechanisms driving chromatin relaxation during the DNA damage response (DDR), and particularly the roles of various histone modifications in regulating chromatin remodelling, however, remain largely unknown.

The linker histone H1 facilitates the folding of chromatin into a more-compact structure^{2,3,11–13}. The disruption of residues within the globular domain of H1, which binds to the DNA entry or exit point of the nucleosome, alters the affinity or mode of binding of H1 to chromatin^{14–16}. Given its critical roles in regulating the higher-order structure to create a permissive chromatin environment for DNA damage repair, H1 is intrinsically linked to the DDR. Indeed, depletion of the linker histone H1 impairs DSB repair^{17–19}. The functions of H1 are largely dependent of its post-translational modifications (PTMs)^{3,20–22}. Although the primary function of H1 is to maintain a compact chromatin structure, it is interesting to note that H1 modifications, such as ubiquitylation, phosphorylation and PARylation, contribute to the DDR mainly by facilitating the recruitment of DSB repair factors, rather than directly affecting chromatin relaxation^{19,23,24}. Thus, fully understanding how H1 modifications influence chromatin accessibility around DSBs is crucial for elucidating the underlying mechanisms.

Deamidation, the removal of an amino group from the side chains of the neutral polar residues asparagine (Asn) and glutamine (Gln),

is a unique PTM because it can be either enzymatically or chemically catalysed²⁵. Recent studies have shown that glutamine amidotransferases (GATs), a family of metabolic enzymes that catalyse the removal of nitrogen from glutamine, are capable of deamidating asparagine residues in key signalling molecules that regulate essential biological processes^{26–28}. The regulation of B cell lymphoma extra-large deamidation has a critical role in the tumour-specific activity of DNA-damaging antineoplastic agents^{29,30}, suggesting that deamidation might also be a functional PTM affecting the DDR; however, the role of histone deamidation, particularly in response to DNA damage, remains entirely unknown. CTPS1, a member of the GAT family, catalyses de novo CTP synthesis^{31,32}, and because of its role in cell proliferation, its inhibitor is currently undergoing clinical trials as a lymphoma treatment^{33–36}. Although recent studies have shown that CTPS1 deficiency induces DNA damage³⁷, the detailed mechanism by which CTPS1 contributes to DNA damage repair remains to be determined.

In this study, we found that H1 deamidation at asparagine residues Asn76 and Asn77 is catalysed by CTPS1 in response to DNA damage. This event leads to increased H1 nucleosome decompaction through the acetylation of the nearby Lys75 residue. These data have thus unveiled a potential therapeutic target for certain cancers.

H1(N76D/N77D) regulates DNA damage repair

Cervical cancer is commonly treated with DNA-damaging chemoradiotherapy, but patients often develop resistance to therapy and there is a high rate of recurrence³⁸. We thus used a HeLa cervical cancer cell line as the model in this study. To investigate the role of H1 PTMs in

¹International Cancer Center, Guangdong Key Laboratory of Genome Instability and Human Disease Prevention, Marshall Laboratory of Biomedical Engineering, Department of Biochemistry and Molecular Biology, Shenzhen University Medical School, Shenzhen, China. ²Shanghai Key Laboratory of Maternal Fetal Medicine, Shanghai First Maternity and Infant Hospital, School of Medicine, Tongji University, Shanghai, China. ³Cancer Institute, Fudan University Shanghai Cancer Center, Department of Oncology, Shanghai Medical College, Fudan University, Shanghai, China. ⁴School of Basic Medical Sciences, Wannan Medical College, Wuhu, China. ⁵Department of Medical Genetics, Peking University Health Science Centre, Beijing, China. ⁶These authors contributed equally: Yuan Tian, Tingting Feng, Jun Zhang. ✉e-mail: zhuweiguo@szu.edu.cn

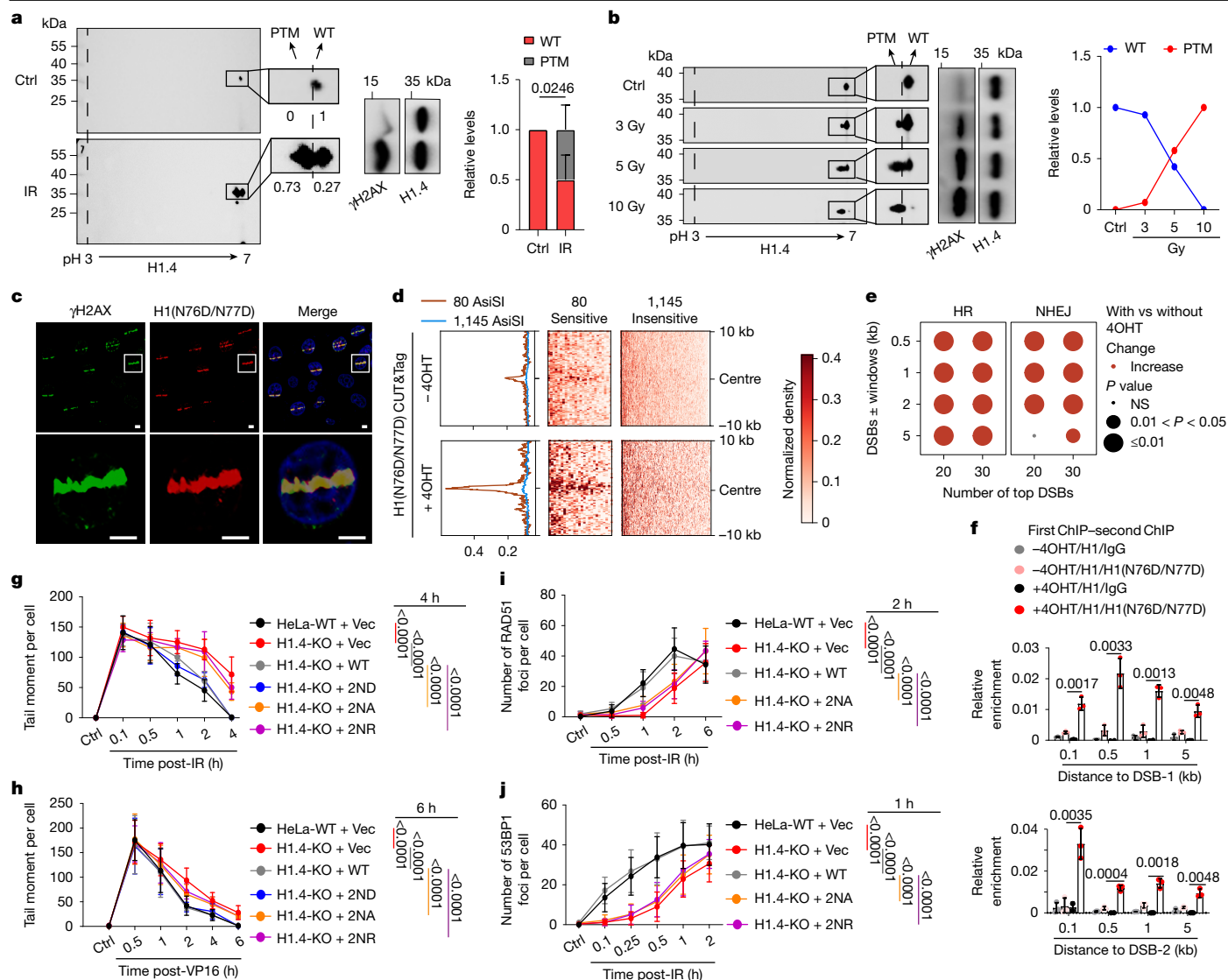


Fig. 1 | H1(N76D/N77D) is required for DNA damage repair. **a**, HeLa cells were exposed to 10 Gy IR and released for 2 min. Histones were analysed by immunoblotting after 2DGE (left) or regular SDS-PAGE (middle). The relative quantification of H1.4 forms (wild type (WT) and PTM) in the representative experiment (under the blot) and three independent experiments (right) is shown. Ctrl, control. **b**, HeLa cells were exposed to the indicated doses of IR and released for 2 min. Histones were analysed by immunoblotting after 2DGE (left) or SDS-PAGE (middle). The relative quantification of H1.4 forms is also shown (right). **c**, HeLa cells were micro-irradiated and analysed by immunofluorescence for γH2AX (green) and H1(N76D/N77D) (red). Scale bars, 5 μm. **d**, U2OS-AsiSI-ER-AID cells were treated with or without 4OHT and subjected to CUT&Tag-seq with anti-H1(N76D/N77D). **e**, Circle plot represents *P* values obtained when CUT&Tag-seq signals for HR and NHEJ DSBs were compared using an increasing

window size. NS, not significant. **f**, U2OS-AsiSI-ER-AID cells were treated with or without 4OHT and subjected to a ChIP-re-ChIP assay with the indicated antibodies. **g, h**, Wild-type or H1.4-knockout (KO) HeLa cells stably expressing wild-type or mutant Flag-H1.4 were analysed by a comet assay at the indicated times post-IR (**g**) or post-VP16 (**h**). Statistical analyses of the tail moment at the indicated time points are shown. Vec, vector. **i, j**, Wild-type or H1.4-KO HeLa cells stably expressing wild-type or mutant Flag-H1.4 were analysed by immunofluorescence for RAD51 (**i**) or 53BP1 (**j**) foci at the indicated times post-IR. Statistical analyses of foci numbers at the indicated time points are shown. Data represent the mean ± s.d. *P* values were calculated using Student's unpaired two-tailed *t*-tests (**a, f–j**) or two-sample Wilcoxon test (**e**). *n* = 3 samples (**a, f**), *n* = 20 or 30 DSBs (**e**) and *n* = 50 cells (**g–j**) from 3 independent experiments.

regulating the DDR, particularly during the early stages, we performed two-dimensional gel electrophoresis (2DGE). In parallel analyses, all three abundant H1 isoforms, H1.2, H1.3 and H1.4, showed a reduction in H1 positive charge in response to ionizing radiation (IR) (Fig. 1a and Extended Data Fig. 1a). Given the critical role of chromatin relaxation in the early stages of the DDR, we next investigated the effect of each major H1 variant on chromatin relaxation. Highly condensed chromatin is less readily extracted into high-concentration sodium chloride solutions, and indeed, more H3 was extracted from cells treated with the DNA-damaging compound etoposide (VP16). In addition, the short interfering RNA (siRNA)-mediated knockdown of H1.4 induced the highest level of H3 release among the knocked down H1 variants (Extended

Data Fig. 1b and Supplementary Fig. 3a), suggesting that H1.4 exerts the strongest chromatin-condensing effects, which is consistent with previous reports³⁹. We further validated the more relaxed chromatin in H1.4-knockout (H1.4-KO) cells (Extended Data Fig. 1c–e). Therefore, we focused on H1.4 as the representative H1 variant in subsequent experiments and observed a clear shift in H1.4 to the positive pole after IR and VP16 exposure in a dose-dependent and time-dependent manner (Fig. 1b and Extended Data Fig. 1f–h). Next, we evaluated the PTMs of the shifted H1 by mass spectrometry and identified the simultaneous deamidation of Asn76 and Asn77 as the most markedly changed deamidation event following DNA damage (Extended Data Fig. 1i–k and Supplementary Fig. 3b–e). The mutation of H1.4 Asn76 and Asn77 to

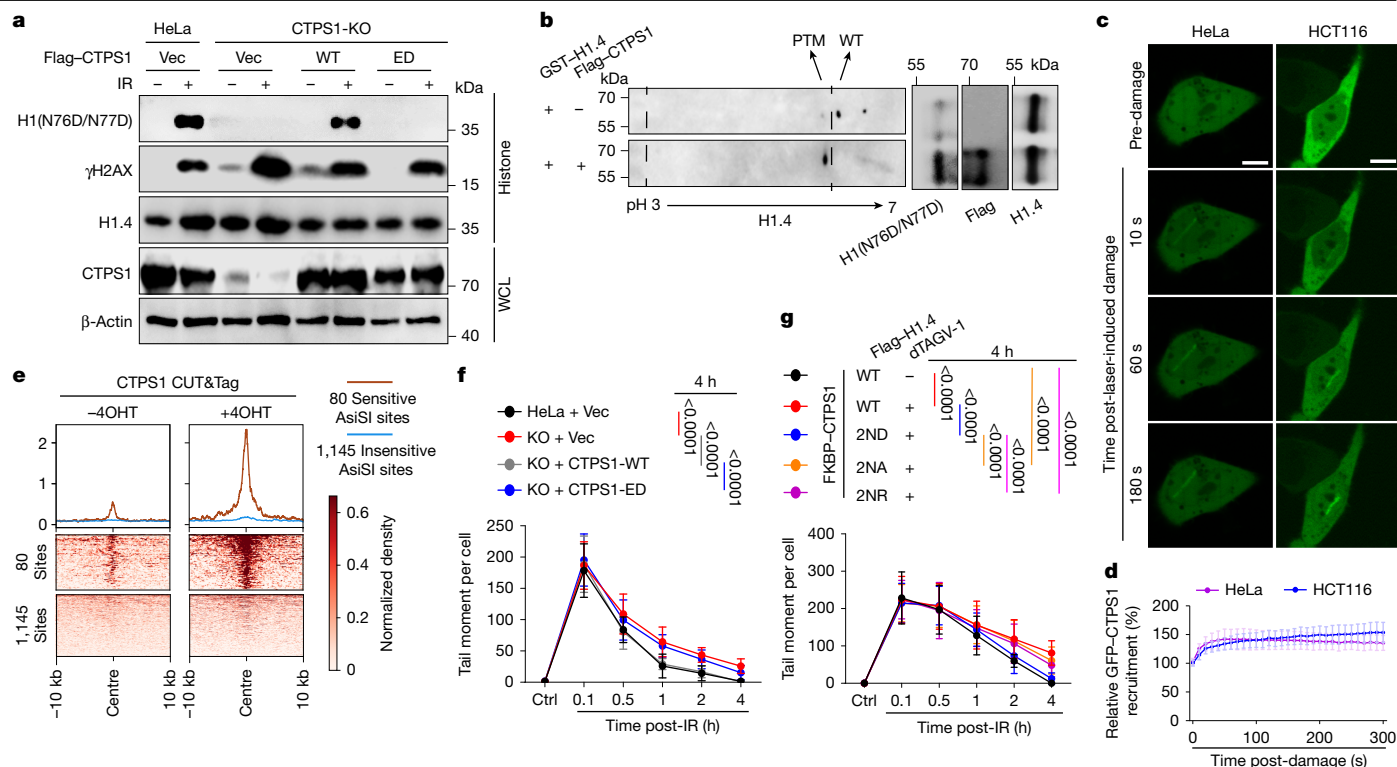


Fig. 2 | CTPS1 deamidates H1 N76/N77 in response to DNA damage.

a, Wild-type or CTPS1-KO HeLa cells stably expressing wild-type or enzymatically dead (ED) Flag-CTPS1 were treated with or without 10 Gy IR. Histones and whole-cell lysates (WCLs) were analysed by immunoblotting. **b**, GST-H1.4 purified from *Escherichia coli* was incubated with or without Flag-CTPS1 purified from HEK293T cells. In vitro deamidation reactions were analysed by immunoblotting after 2DGE (left) and SDS-PAGE (right). **c,d**, Representative cells (**c**) and quantification (**d**) of GFP signals in HeLa and HCT116 cells that were transfected with GFP-CTPS1 and exposed to laser micro-irradiation. Scale bars, 5 μ m. **e**, U2OS-AsiSI-ER-AID cells were treated

alanine residues (H1.4-2NA) almost completely abolished the reduction in positive charge on H1.4 during the DDR (Extended Data Fig. 1l).

To directly examine the levels of H1 Asn76 and Asn77 deamidation to aspartic acid (H1(N76D/N77D)), we generated a site-specific antibody targeting H1(N76D/N77D) (Extended Data Fig. 2a–d). We established a quadruple-knockout H1 variant HeLa cell line (H1.1–H1.4-KO; referred to as 4KO) and found that H1(N76D/N77D) signals were much weaker in 4KO cells than in wild-type cells after DNA damage (Extended Data Fig. 2e,f). H1(N76D/N77D) levels increased in response to IR-induced, VP16-induced and laser micro-irradiation-induced DNA damage (Fig. 1c and Extended Data Fig. 2g,h). We further verified the enhanced levels of H1(N76D/N77D) around DSBs using a U2OS-AsiSI-ER-AID cell line, in which site-specific DSBs can be induced by 4-hydroxytamoxifen (4OHT). Cleavage under targets and tagmentation sequencing (CUT&Tag-seq), chromatin immunoprecipitation with quantitative PCR (ChIP-qPCR), and ChIP-re-ChIP analyses all revealed the enrichment of H1(N76D/N77D) at the 80 sensitive damaged sites prone to both homologous recombination and non-homologous end-joining (NHEJ) repair pathways (Fig. 1d–f and Extended Data Fig. 2i). Hydroxyurea-mediated DNA replication stress and long-release period after exposure to ultraviolet radiation C also increased H1(N76D/N77D) levels, probably due to subsequent DSB formation, whereas metabolic or inflammatory stresses, which do not induce DSBs, had no effect (Extended Data Fig. 2j,k). Increased H1(N76D/N77D) is thus a widespread biological phenomenon that occurs in response to DNA damage.

We next explored the role of H1(N76D/N77D) in DNA damage repair. Comet assays showed that compared with H1.4-KO cells, which

with or without 4OHT and subjected to CUT&Tag-seq with anti-CTPS1. **f**, Wild-type or CTPS1-KO HeLa cells stably expressing wild-type CTPS1 or CTPS1-ED were analysed by a comet assay at the indicated times after IR. Statistical analyses of the tail moment at 4 h post-IR are shown. **g**, H1.4-KO HeLa cells stably expressing wild-type or mutant Flag-H1.4 were modified to express FKBP-CTPS1, treated with dTAGV-1 for 3 h, and then exposed to IR. Cells were analysed by a comet assay at the indicated times after IR. Statistical analyses of the tail moment at 4 h post-IR are shown. Data represent the mean \pm s.d. P values were calculated using Student's unpaired two-tailed t-tests (f,g). n = 8 (d) or n = 50 (f,g) cells from 3 independent experiments.

exhibited severely impaired repair efficiency, knockout cells stably expressing wild-type H1.4 or H1.4 with Asn76 and Asn77 mutated to aspartic acid to mimic deamidation (H1.4-2ND) demonstrated improved DNA repair. By contrast, only a slight recovery in tail moment clearance was observed in cells expressing H1.4-2NA or H1.4-2NR (with mutation of Asn76 and Asn77 to arginine), designed to disrupt deamidation (Fig. 1g,h and Supplementary Fig. 4a–e).

Given that chromatin accessibility facilitates the recruitment of repair factors to DSB sites, we also investigated the foci formation of two typical repair factors: RAD51 (for homologous recombination) and 53BP1 (for NHEJ). As expected, compared with cells expressing wild-type H1.4, H1.4-KO cells expressing an empty vector, H1.4-2NA or H1.4-2NR cells contained reduced numbers of RAD51 and 53BP1 foci, reflecting the decreased efficiency of both repair pathways (Fig. 1i,j and Supplementary Fig. 4f,g). Together, these results confirm that H1 deamidation is essential for DNA damage repair.

CTPS1 deamidates H1 after DNA damage

The human genome encodes 11 GATs²⁵, but only CTPS1 knockdown inhibited the level of H1(N76D/N77D) induced by IR exposure (Extended Data Fig. 3a). We also found that the reintroduction of wild-type CTPS1 efficiently rescued the H1(N76D/N77D) levels in CTPS1-KO cells, whereas enzymatically dead (C399A/H526A/E528A; hereafter termed ED)⁴⁰ CTPS1 had no effect (Fig. 2a and Supplementary Fig. 5a–c). As Cys399 is mainly responsible for the GAT activity of CTPS1, we also observed a disruption to the H1(N76D/N77D) increase in CTPS1(C399A)-expressing

cells (Supplementary Fig. 5d), confirming that the GAT activity of CTPS1 is essential for H1(N76D/N77D).

We next established an inducible CTPS1 degradation system (FKBP–CTPS1) in HeLa cells. Consistent with previous findings, CTPS1 degradation resulted in a diminished IR-induced increase in H1(N76D/N77D) levels (Extended Data Fig. 3b). Validating these findings, we detected an interaction between CTPS1 and H1.4 following IR exposure (Extended Data Fig. 3c,d). In addition, although CTPS1 interacted with all major H1 variants, the most enhanced interaction upon DNA damage was that between CTPS1 and H1.4 (Extended Data Fig. 3e). We also confirmed that histidine-tagged CTPS1 (His–CTPS1) interacted directly with glutathione *S*-transferase (GST)-tagged H1.4 (GST–H1.4), but not with GST alone or core histones (Extended Data Fig. 3f,g). To confirm the function of CTPS1 as a bona fide deamidase, we performed *in vitro* deamidation assays. Compared with the no-enzyme control, wild-type CTPS1, but not CTPS1-ED, caused H1.4 to shift towards the positive pole and an increase in H1(N76D/N77D) levels (Fig. 2b and Extended Data Fig. 3h). Finally, we predicted the interaction between the enzymatic pocket of CTPS1 and H1.4 Asn76 and Asn77 (Supplementary Fig. 5e).

Having established a critical role for CTPS1 in H1(N76D/N77D), we hypothesized that this enzyme also contributes to DNA damage repair. We first observed an enrichment of CTPS1 on chromatin following IR or VP16 treatment (Extended Data Fig. 3i,j). We then detected clear CTPS1 enrichment at laser micro-irradiation-induced, AsiSI-induced and FokI-induced DNA damage sites (Fig. 2c–e and Extended Data Fig. 3k–m). This CTPS1 recruitment to DSBs was abolished in 4KO cells but not in H1.4-only knockout cells, which we attributed to the interaction between CTPS1 and other H1 variants (Extended Data Fig. 3n–p and Supplementary Fig. 5f–h). We also found that CTPS1 phosphorylation at Ser575 was induced by DNA damage, a modification essential for CTPS1 recruitment to DSB sites (Supplementary Fig. 5i–k). Overall, we posited that CTPS1 is recruited to DSB sites to mediate H1(N76D/N77D).

We subsequently investigated the role of CTPS1 in DNA damage repair. As expected, CTPS1 knockout or knockdown decreased the repair efficiency of DNA damage induced by IR or VP16. Expression of wild-type CTPS1, but not CTPS1-ED, rescued the inhibition of DNA repair in CTPS1-KO cells (Fig. 2f, Extended Data Fig. 4a and Supplementary Fig. 6a–d). Moreover, expression of wild-type CTPS1, but not CTPS1-ED, rescued the CTPS1-knockdown-induced decrease in repair in both pDR–GFP (for homologous recombination) and pEJ5–GFP (for NHEJ) U2OS reporter cells (Extended Data Fig. 4b and Supplementary Fig. 6e–i). Consistent with this finding, CTPS1-KO cells inhibited the formation of RAD51 and 53BP1 foci following DNA damage, which was rescued by wild-type CTPS1 but not by CTPS1-ED (Extended Data Fig. 4c,d and Supplementary Fig. 6j,k). All these data suggested that the mechanism by which CTPS1 modulates DNA damage repair is enzymatic activity dependent. Although the addition of CTP restored CTP levels in the CTPS1-KO cells, DNA repair efficiency was not restored to basal levels, indicating that the role of CTPS1 in the DDR is independent of CTP synthesis activity (Extended Data Fig. 4e–g and Supplementary Fig. 7a,b).

We further explored the role of H1(N76D/N77D) in the mechanism by which CTPS1 mediates DNA repair. Compared with cells expressing wild-type H1.4, CTPS1-degraded or CTPS1-knockdown cells expressing H1.4-2ND led to an improved DNA repair capacity, whereas H1.4-2NA or H1.4-2NR expression was markedly less effective (Fig. 2g, Extended Data Fig. 4h–k and Supplementary Fig. 7c–g). In addition, both CTPS1 degradation and H1.4-KO in cells led to defects in DNA repair efficiency, with no further defects observed when both CTPS1 and H1.4 were simultaneously disrupted (Supplementary Fig. 8a–f). These findings confirmed that the role of CTPS1 in DNA damage repair is primarily dependent on H1, and that H1(N76D/N77D) is the functional modification site that regulates CTPS1-mediated DNA damage repair.

H1(N76D/N77D) is a prerequisite for H1K75ac

On the basis of the role of H1 as a linker DNA-binding histone, we hypothesized that H1(N76D/N77D) is associated with chromatin relaxation during the DDR. As expected, compared with cells expressing wild-type H1.4, cells expressing H1.4-2NA or H1.4-2NR showed diminished chromatin relaxation following DNA damage. Although H1.4-2ND expression promoted nucleosome relaxation after DNA damage, it did not induce a more relaxed chromatin state under physiological conditions (Fig. 3a and Extended Data Fig. 5a), indicating that other mechanisms are involved after H1(N76D/N77D).

Our mass spectrometry analysis revealed that the Lys75 residue adjacent to Asn76 is also acetylated (Extended Data Fig. 5b). We therefore generated specific antibodies targeting H1K75 acetylation (H1K75ac) or simultaneous modifications of these three sites (H1K75ac2ND) (Extended Data Fig. 5c–f). Similar to H1(N76D/N77D), the levels of H1K75ac and H1K75ac2ND increased immediately after IR or VP16 exposure (Fig. 3b and Extended Data Fig. 5g). We further confirmed the induction of H1K75ac and H1K75ac2ND in U2OS–AsiSI–ER–AID cells and micro-irradiated cells (Extended Data Fig. 5h–j). Collectively, these data show that H1K75ac and H1K75ac2ND increase in response to DNA damage.

We then explored the relationship between H1(N76D/N77D) and H1K75ac. HeLa cells transfected with wild-type H1.4 or H1.4(K75R) (an arginine substitution mutant of Lys75) showed only minimal differences in H1.4 charge status in response to DNA damage (Extended Data Fig. 6a), suggesting that H1K75ac does not affect H1(N76D/N77D). By contrast, H1K75ac was induced by IR in H1.4 and H1.4-2ND cells, but not in H1.4-2NA or H1.4-2NR cells (Fig. 3c and Extended Data Fig. 6b). Consistent with this finding, CTPS1-KO cells did not show increased levels of H1K75ac or H1K75ac2ND following IR or micro-irradiation (Fig. 3d,e and Extended Data Fig. 6c).

We next examined the influence of H1K75ac and H1K75ac2ND on DNA damage repair efficiency. H1.4-KR, or the triple mutants H1.4-RAA and H1.4-RRR (in which Lys75, Asn76 and Asn77 were substituted to alanine or arginine), compromised DNA break repair compared with wild-type H1.4. By contrast, H1.4-KQ (a glutamine substitution mutant of Lys75) and H1.4-QDD did not result in defective repair (Fig. 3f–i and Supplementary Fig. 9a–f). Together, we conclude that H1(N76D/N77D) is a prerequisite for H1K75ac.

p300 acetylates H1K75 after DNA damage

Next, we sought to identify the histone acetyltransferases (HATs) responsible for H1K75ac. Knockdown of several typical HATs showed that IR-induced H1K75ac was specifically inhibited only when p300 was targeted (Extended Data Fig. 7a); the expression of p300 HAT rescued H1K75ac levels, whereas enzymatically dead (E1399A) p300 HAT had no such effect (Fig. 4a). Next, we confirmed that the interaction between p300 and H1.4 was enhanced in IR-treated cells, and there was a direct interaction between His–H1.4 and the HAT-CH2 domain of p300 *in vitro* (Fig. 4b,c and Extended Data Fig. 7b,c). We saw a band representing p300 HAT and H1.4 at a higher molecular weight than the band representing p300 HAT alone in native PAGE (Extended Data Fig. 7d). In addition, GFP–p300 HAT colocalized with the FokI–mCherry foci, suggesting that p300 was recruited to DSBs to catalyze H1K75ac (Extended Data Fig. 7e).

Results from an *in vitro* acetylation assay showed that the catalytic core of p300 was sufficient to acetylate H1K75 (Fig. 4d). However, GST–p300 HAT had no such effect on His–H1.4(K75R) acetylation levels (Extended Data Fig. 7f). We further noted that the inhibited DNA repair efficiency induced by p300 knockdown was improved by H1.4-KQ, but not by H1.4-KR (Extended Data Fig. 7g–j and Supplementary Fig. 10a–h). These data indicate that p300-mediated H1K75ac participates in DNA damage repair.

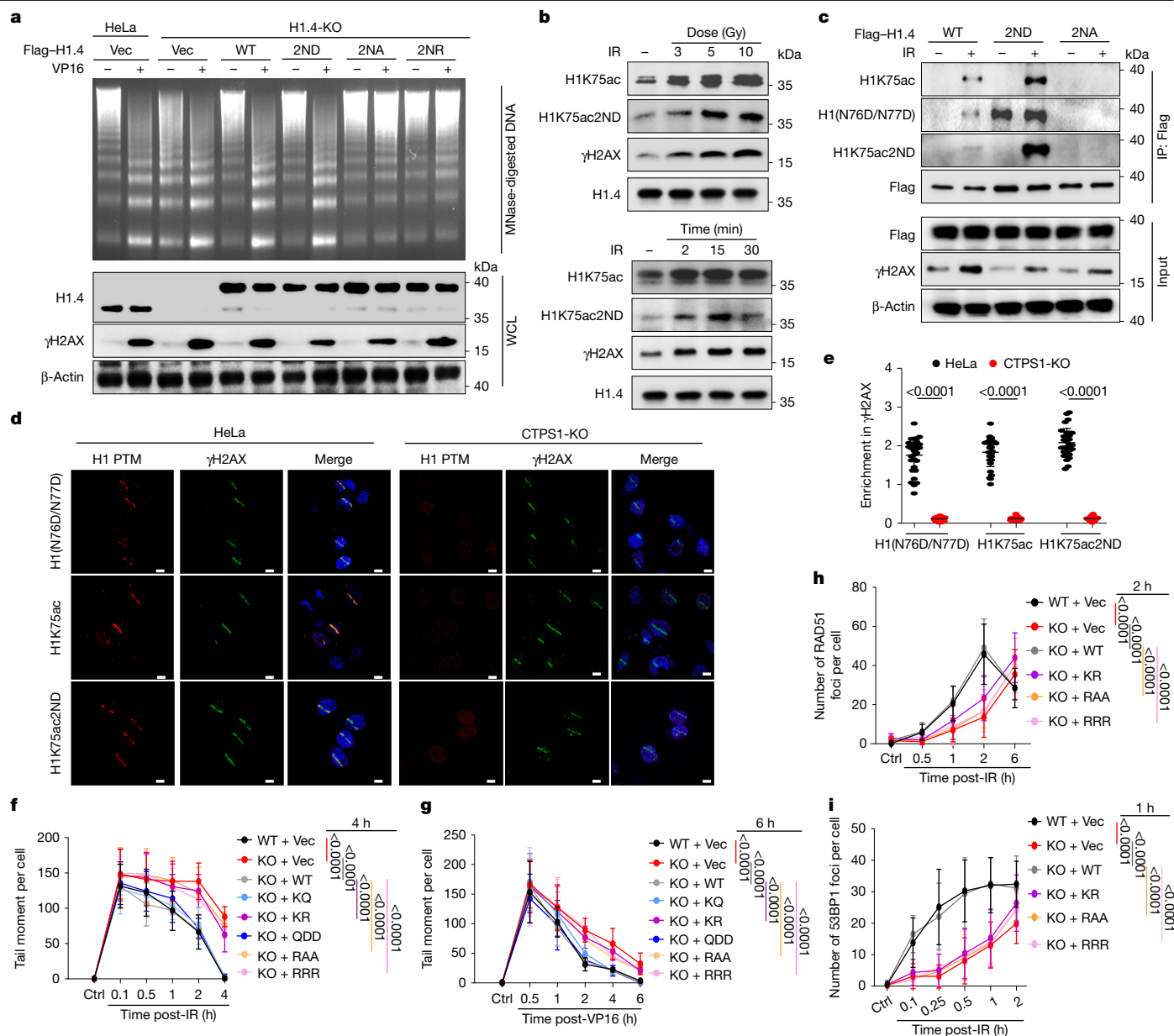


Fig. 3 | H1(N76D/N77D) is a prerequisite for H1K75ac. **a**, Chromatin fractions were extracted from wild-type or H1.4-KO HeLa cells stably expressing wild-type or mutant Flag-H1.4 and analysed by an MNase-sensitivity assay (top). WCLs were analysed by immunoblotting (bottom). **b**, HeLa cells were exposed to the indicated doses of IR and released for 2 min (top) or exposed to 10 Gy IR and released for the indicated times (bottom). Histones were extracted for immunoblotting using anti-H1K75ac or anti-H1K75ac2ND antibodies. **c**, H1.4-KO HeLa cells stably expressing wild-type or mutant Flag-H1.4 were exposed to IR. WCLs were extracted, immunoprecipitated using anti-Flag and analysed by immunoblotting. **d, e**, Wild-type or CTSP1-KO HeLa cells were analysed by immunofluorescence for H1 PTM (red) and γH2AX (green) at 5 min

post-micro-irradiation. Representative images (**d**) and quantification (**e**) of 30 cells are shown. Scale bars, 5 μm. **f, g**, Wild-type or H1.4-KO HeLa cells stably expressing wild-type or mutant Flag-H1.4 were analysed by a comet assay at the indicated times post-IR (**f**) or post-VP16 (**g**). Statistical analyses of the tail moment at the indicated time points post-treatment are shown. **h, i**, Wild-type or H1.4-KO HeLa cells stably expressing wild-type or mutant Flag-H1.4 were analysed by immunofluorescence for RAD51 (**h**) or 53BP1 (**i**) foci at the indicated times post-IR. Statistical analyses of foci numbers at the indicated time points post-IR are shown. Data represent the mean ± s.d. *P* values were calculated using Student's unpaired two-tailed *t*-tests (**e–i**). *n* = 30 (**e**) and *n* = 50 (**f–i**) cells from 3 independent experiments.

We next explored the role of H1(N76D/N77D) in p300 recruitment to DNA damage sites. Consistent with the effects of H1(N76D/N77D) inhibition, CTSP1 deficiency abolished the recruitment of p300 to DSBs or damaged chromatin. This defect was rescued upon overexpression of H1.4-2ND, but not H1.4, H1.4-2NA or H1.4-2NR (Fig. 4e and Extended Data Fig. 8a–c). In addition, Flag-H1.4 interacted less with p300 in CTSP1-deficient cells following IR treatment, and Flag-H1.4-2ND expression enhanced the binding of p300 to H1.4, whereas almost no Flag-H1.4-2NA or Flag-H1.4-2NR binding with p300 was detected (Fig. 4f, g and Extended Data Fig. 8d). A GST pull-down assay confirmed

an enhanced interaction between GST-p300 HAT and His-H1.4-2ND, which further facilitated the induction of H1K75ac by GST-p300 HAT (Fig. 4h and Extended Data Fig. 8e). Moreover, molecular docking simulations indicated that deamidated H1.4 might be a preferential substrate for p300 HAT due to the closer spatial proximity of the interacting amino acids (Extended Data Fig. 8f).

By contrast, after knocking down p300, we saw similar patterns of CTSP1 chromatin recruitment and H1(N76D/N77D) levels after DNA damage, and also no differences in the binding of CTSP1 to wild-type H1.4, H1.4-KQ or H1.4-KR (Extended Data Fig. 8g–j). We thus

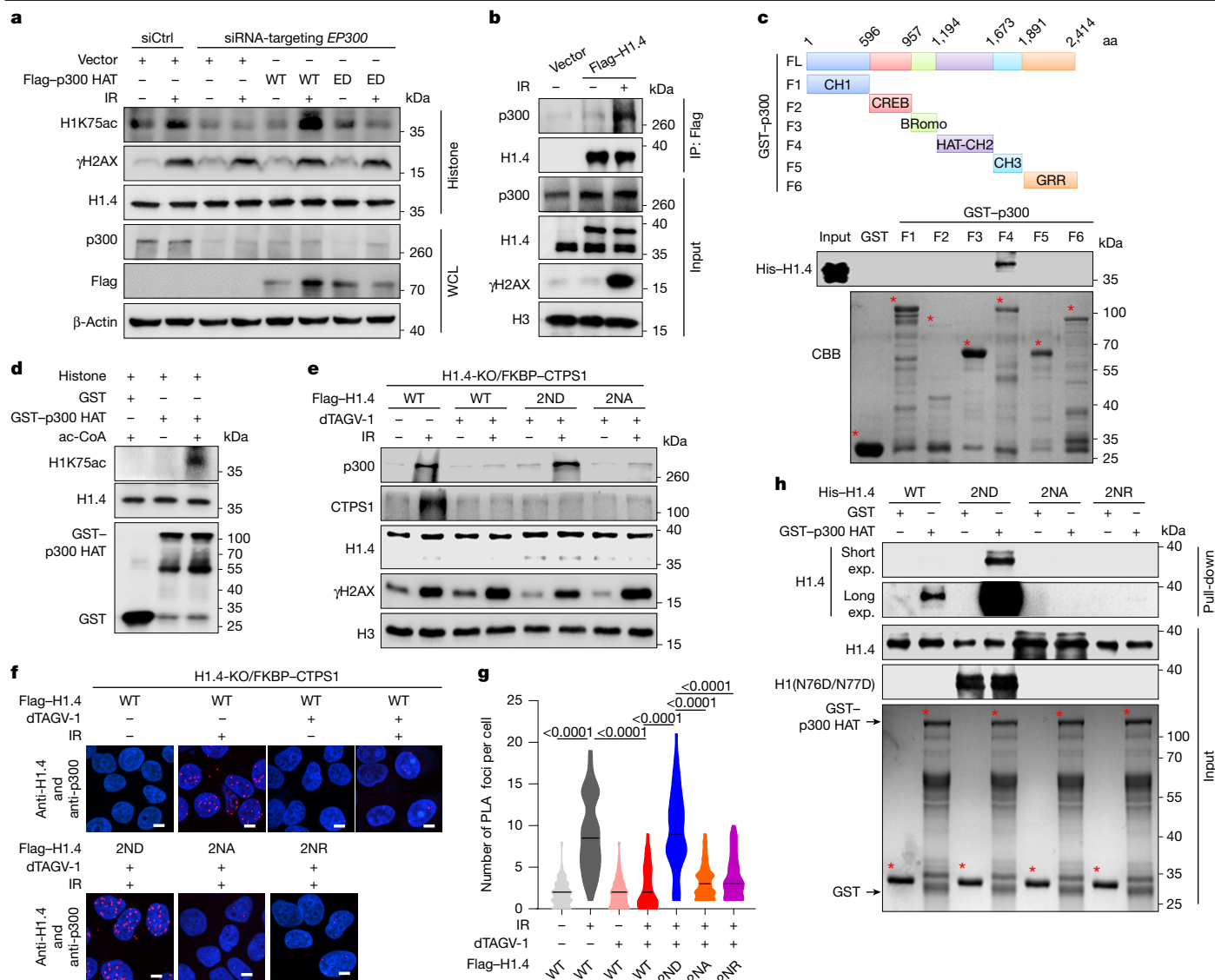


Fig. 4 | H1(N76D/N77D) promotes p300 binding to chromatin and H1K75ac.

a, HeLa cells were transfected with the indicated siRNAs, followed by plasmid transfection for 48 h, and exposed or not to 10 Gy IR. Histones and WCLs were analysed by immunoblotting. **b**, HeLa cells were transfected with Flag-H1.4 for 48 h and exposed or not to 10 Gy IR. WCLs were extracted, immunoprecipitated using anti-Flag and analysed by immunoblotting. **c**, Recombinant GST or GST-p300 fragments (top) were incubated with His-H1.4 for GST pull-down assays (bottom). Coomassie brilliant blue (CBB) staining is shown. The asterisks indicate specific protein bands. FL, full-length. **d**, GST or GST-p300 HAT was subjected to in vitro acetylation assays using free histones extracted from HeLa cells. **e–g**, H1.4-KO HeLa cells stably expressing wild-type or mutant

Flag-H1.4 were modified to express FKBP-CTPS1, treated with dTAGV-1 for 3 h, and exposed or not to 10 Gy IR. Chromatin was analysed by immunoblotting (**e**), or proximity ligation assay was performed using anti-H1.4 and anti-p300, with representative images (**f**) and quantification of 50 cells (**g**) shown. Scale bars, 5 μm. **h**, Recombinant GST-p300 HAT protein was incubated with His-H1.4, His-H1.4-2ND, His-H1.4-2NA or His-H1.4-2NR for the GST pull-down assay (top). CBB staining is also shown (bottom). The asterisks indicate specific protein bands. Exp., exposure. Data represent the mean ± s.d. *P* values were calculated using Student's unpaired two-tailed *t*-tests (**g**). *n* = 50 cells from 3 independent experiments (**g**).

concluded that H1K75ac does not affect CTPS1 recruitment to DSB sites or its binding to H1 following DNA damage.

H1K75ac promotes chromatin relaxation

We next investigated whether H1K75ac and H1K75ac2ND are involved in chromatin relaxation. We found that cells expressing H1.4-KR, H1.4-RAA and H1.4-RRR were more resistant to micrococcal nuclease (MNase) digestion and released lower levels of H3 than wild-type H1.4- cells, whereas H1.4-KQ and H1.4-QDD cells showed more relaxed chromatin (Fig. 5a and Extended Data Fig. 9a,b). We also performed the assay for transposase-accessible chromatin with high-throughput sequencing (ATAC-seq) and found that 4OHT induced a more accessible signal

near the AsiSI site (Fig. 5b). In addition, the relaxed regions were highly associated with H1 deamidation and acetylation, as well as with CTPS1-enriched regions (Fig. 5c and Supplementary Fig. 11a). Moreover, H1.4-KO U2OS-AsiSI-ER-AID cells transfected with an H1.4-RAA plasmid exhibited disrupted chromatin relaxation following 4OHT treatment (Fig. 5b). These findings indicate that sequential H1(N76D/N77D) and H1K75ac promote chromatin relaxation during the DDR.

We next determined the roles of CTPS1 in H1-mutation-mediated chromatin remodelling. The overexpression of CTPS1, but not CTPS1-ED, rescued the CTPS1-knockdown-induced defects in chromatin relaxation (Extended Data Fig. 9c and Supplementary Fig. 11b). Following CTPS1 downregulation, no improvement in chromatin relaxation was observed in H1.4-expressing, H1.4-2NA-expressing or H1.4-2NR-expressing

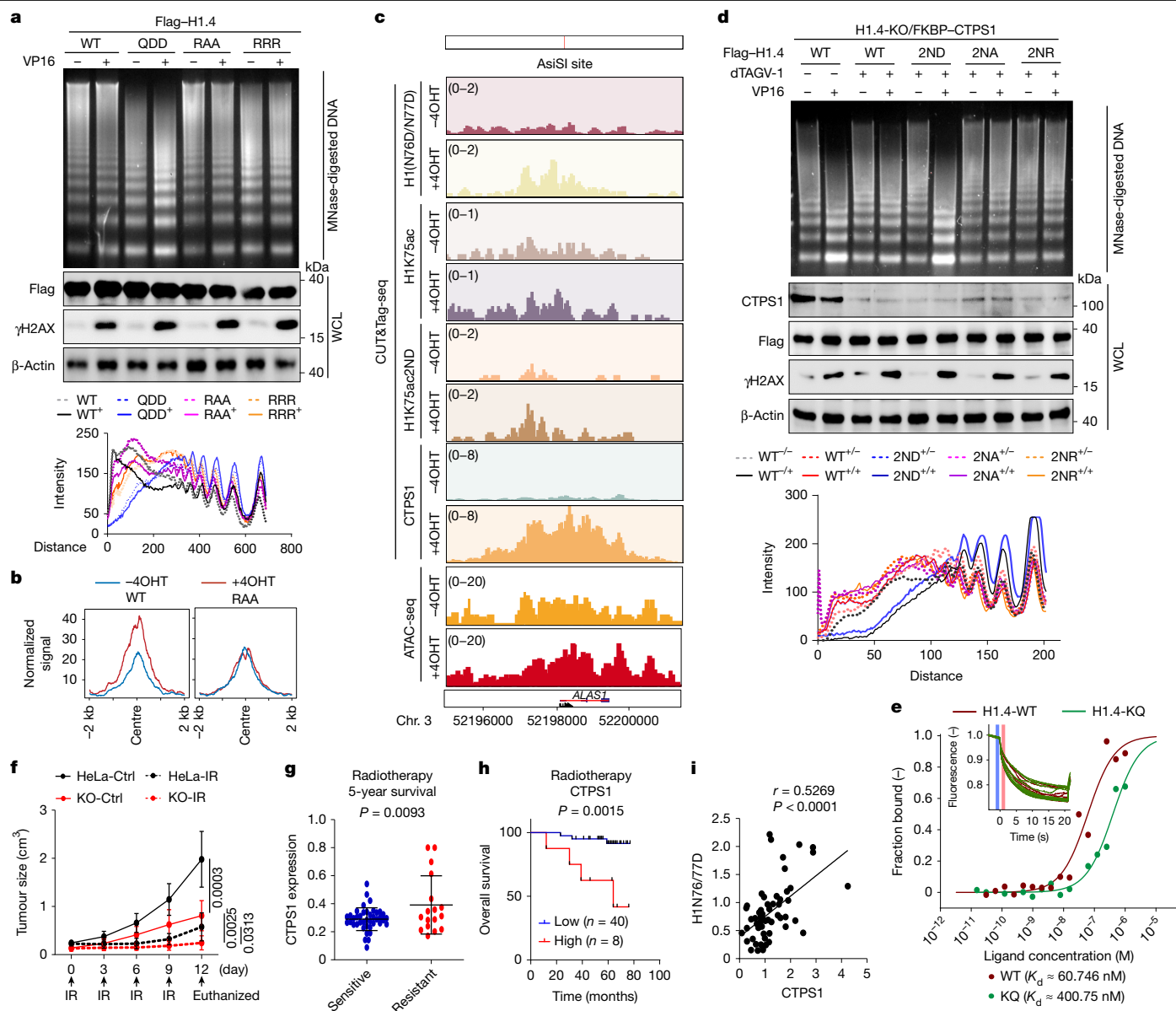


Fig. 5 | Sequential H1(N76D/N77D) and H1K75ac promote chromatin relaxation and maintain genome stability. a, Chromatin fractions or WCLs were extracted from H1.4-KO HeLa cells that were transfected with the indicated plasmids, and analysed by an MNase assay (top) or immunoblotting (middle), and the intensity of each lane was quantified (bottom). **b**, H1.4-KO U2OS-AsiSI-ER-AID cells were transfected with wild-type H1.4 or H1.4-RAA plasmids and treated with or without 4OHT. Cells were subjected to ATAC-seq. Normalized signals of 80 sensitive DSB sites were plotted. **c**, U2OS-AsiSI-ER-AID cells were treated with or without 4OHT and subjected to ATAC-seq or CUT&Tag-seq with the indicated antibodies. Normalized signals of a representative DSB site is shown. **d**, H1.4-KO HeLa cells expressing wild-type or mutant Flag-H1.4 were modified to express FKBP-CTPS1, and treated with or without VP16 after being treated with or without dTAGV-1 for 3 h. Chromatin fractions or WCLs were analysed by an MNase assay (top) or immunoblotting (middle).

cells, but the levels of chromatin relaxation were increased in cells expressing H1.4-2ND (Fig. 5d and Extended Data Fig. 9d). We also found less transposase-accessible chromatin around DSB sites in CTPS1-knockdown cells (Extended Data Fig. 9e). Similarly, p300-deficient cells exhibited increased chromatin compaction compared with control cells, which was prevented by p300 HAT over-expression (Supplementary Fig. 11c). Moreover, rescued H1.4-KQ, but

The intensity of each lane was also quantified (bottom). **e**, The affinity between purified His-H1.4 or His-H1.4-KQ proteins and synthesized DNAs was analysed by an MST assay. **f**, Wild-type or CTPS1-KO HeLa cells were injected into nude mice, with or without (Ctrl) exposure to IR ($n = 6$ per group). Growth curves of xenografts are shown. **g**, Quantification of CTPS1 expression in cervical cancer tissues ($n = 58$). Blue indicates sensitive patients who survived 5 years after radiotherapy, and red denotes resistant patients who had died within 5 years of radiotherapy. **h**, Overall survival of patients with survival information ($n = 48$). Blue indicates low CTPS1 expression, red denotes high CTPS1 expression. **i**, Correlation of CTPS1 and H1(N76D/N77D) expression in cervical tumour and para-tumour tissues ($n = 57$). Data represent the mean \pm s.d. (**f,g**). P values were calculated using Student's unpaired two-tailed t -tests (**f,g**), log-rank (Mantel-Cox) test (**h**) or Pearson r test (**i**).

not H1.4 or H1.4-KR, expression abolished the increase in chromatin compaction induced by p300 knockdown (Extended Data Fig. 9f,g).

We then demonstrated that the interaction between H1.4 and DNA was approximately six times stronger than that between H1.4-KQ and DNA (Fig. 5e). Lys75, Asn76 and Asn77 form one of the two core binding domains for the interaction of H1.4 with linker DNA. H1.4-QDD showed a more relaxed mode of H1.4 and linker DNA binding, verifying our

finding that H1K75ac2ND leads to a lower affinity of acetylated H1 for DNA and therefore chromatin relaxation (Supplementary Fig. 11d). These results demonstrate that sequential CTPS1-mediated H1(N76D/N77D) and p300-mediated H1K75ac facilitate chromatin relaxation upon DNA damage.

We also investigated the importance of PARylation in chromatin relaxation and found no regulatory crosstalk between PARP1 and H1(N76D/N77D) or H1K75ac after DNA damage (Supplementary Fig. 11e–g), indicating that H1 deamidation and PARP1 are two independent pathways during the DDR. Although PARP1 mainly affects core histone compaction^{41,42}, H1 deamidation may function in moderating the affinity between H1 and linker DNA and thus condensing the nucleosome array.

CTPS1 is a radiotherapy sensitizer

Disturbed chromatin relaxation leads to genome instability and chromosome abnormalities, which in turn cause tumour cell death in response to radiotherapy. We found that cells stably expressing H1.4-2NR, H1.4-2NA, H1.4-KR, H1.4-RAA or H1.4-RRR displayed more chromosome breaks after DNA damage (Extended Data Fig. 10a and Supplementary Fig. 12a). Similarly, CTPS1-KO cells exhibited more severe chromosome defects when treated with IR (Extended Data Fig. 10b and Supplementary Fig. 12b), demonstrating that the chromatin relaxation induced by sequential H1(N76D/N77D) and H1K75ac is required for genome stability.

Consistent with these genome stability results, we found that cells stably expressing defective H1.4 mutants showed an increased sensitivity to DNA damage (Extended Data Fig. 10c,d and Supplementary Fig. 12c,d). 4KO cells exhibited slower growth without DNA damage and a greater sensitivity to IR (Supplementary Fig. 12e–g). We also investigated the contribution of CTPS1 to the radiotherapy sensitivity of cells. Although the proliferation of CTPS1-KO cells without DNA damage was inhibited, they showed significantly compromised clonogenic survival following VP16 or IR treatment that was mainly independent of CTP levels (Extended Data Fig. 10e–g and Supplementary Fig. 12h–m).

Next, we explored the role of CTPS1 and H1 deamidation in tumour growth *in vivo*. Induction of H1(N76D/N77D) was disrupted in H1.4-RAA and H1.4-RRR xenografts, leading to inhibited tumour growth after treatment with IR (Supplementary Fig. 13a–d). Similarly, IR suppressed the growth of CTPS1-KO xenografts to a greater extent than that of wild-type xenografts (Fig. 5f and Extended Data Fig. 10h–j). In addition, a high-CTPS1-expressing cancer cell line exhibited greater resistance to radiotherapy than a low-CTPS1-expressing cancer cell line (Supplementary Fig. 13e–g). These data suggest that CTPS1 has a potential role as a radiosensitizer for cancer therapy.

We finally determined the pathological relevance of CTPS1 in clinical cancer specimens. Of note, a cervical carcinoma tissue microarray isolated from patients before radiotherapy showed that CTPS1 was upregulated in those with subsequent radiotherapy resistance (Fig. 5g and Extended Data Fig. 10k), and overall survival was poorer in patients expressing high CTPS1 levels (Fig. 5h). Another cohort showed a positive correlation between CTPS1 and H1(N76D/N77D) in cervical carcinomas tested after radiotherapy (Fig. 5i and Extended Data Fig. 10l). Analysis of public databases showed that high expression of CTPS1 was also associated with poorer overall survival in patients with DNA damage-based chemotherapy-treated lung and gastric cancer than in the total patient population (Supplementary Fig. 13h). We thus propose that CTPS1 might be a potential target to improve cancer radiotherapy (Extended Data Fig. 10m).

Discussion

Recent spectrometric analyses have revealed an extensive number of H1 PTMs that may be linked to chromatin structure and dynamics^{11,43}.

With almost identical sequences, PTMs in the globular domain of the somatic H1 variants are highly conserved, whereas PTMs in the tails of H1 variants vary substantially due to differences in tail sequences¹¹. Therefore, modifications in the globular domain of H1 typically have fundamental roles in various biological processes^{22,23,44}. The disruption of residues within the globular domain affects the affinity or modality of H1 binding to chromatin^{14–16,44}. These findings, together with our discovery that the K75Q mutation of H1 decreases chromatin compaction, support the importance of modifications in the H1 globular domain in regulating chromatin relaxation.

Various histone PTMs at DSBs can provide platforms for or directly lead to chromatin relaxation. In the latter case, histone acetylation reduces the number of charge-dependent histone–DNA interactions, thereby inducing chromatin decompaction⁴⁵. Several histone acetylation sites involved in DNA damage have been reported^{8,46}; however, the mechanisms by which histone acetylation is initiated in the early stages of the DDR have only recently begun to garner attention from researchers⁶. In the present study, we not only identified an H1 acetylation site (H1K75ac) that facilitates chromatin relaxation in response to DNA damage but also revealed the permissive conditions for this acetylation event. Previous studies have shown that one type of histone modification can be determined by another type of modification on neighbouring residues. For example, H3K4 methylation promotes the binding of the nucleosomal acetyltransferase complex to acetylate histone H3 at Lys14 (refs. 47–50). On the basis of our results, we propose a similar sequential regulatory model for histone modification crosstalk that is mediated by enhancing the interactions of ‘writers’ with modified histones.

Deamidation rates are controlled by the primary protein sequence, with deamidation occurring increasingly more readily in the sequence order NG > NS > NN > NT > NH⁵¹. Accordingly, we found that Asn76 and Asn77 of H1, which are adjacent to Ser78, comprise the only deamidation hotspot in the H1 globular domain sequence. Although the surrounding sequence and cellular environment could accelerate the deamidation rate, non-enzymatic reactions generally vary between 1 and 500 days for asparagine and 500 and 17,900 days for glutamine⁵². Although these reactions are evidently too slow to function as a stress response, they have been recognized to be a molecular clock of ageing^{52,53}. Compared with non-enzymatic reactions, the protein deamidation catalysed by enzymes is generally rapid and tightly regulated in response to various stimuli^{54–56}. In our study, H1 was deamidated by CTPS1 several minutes after DNA damage, suggesting that this enzymatic deamidation is a rapid-response PTM involved in maintaining cellular homeostasis.

Protein deamidation is generally considered to be associated with a loss of biological function⁵⁴. So far, only a small subset of proteins in prokaryotes and mammalian cells has been shown to gain function after deamidation. Initial studies have shown that the glutamine deamidation of Ras homologue family member A leads to G protein activation^{57,58}. Others have revealed that the deamidation of various signalling molecules facilitates transcriptional activation and immune evasion^{26–28}. Here we revealed that CTPS1-catalysed H1(N76D/N77D) may induce a conformational change favourable for p300 binding in response to DNA damage, offering new evidence that deamidation is also an enzyme-catalysed PTM with an essential role in cellular processes. The effects of enzymatic action on restoring asparagine or glutamine from aspartic acid or glutamic acid residues remain to be clarified in future studies.

The role of CTPS1 was initially characterized in the blood system^{34,36,37}, but recent studies have provided evidence for a broader role for CTPS1 across various cancers^{35,59,60}. CTPS1 is reportedly involved in the DNA replication stress caused by pyrimidine deficiency^{37,60}, but the mechanisms by which CTPS1 regulates DNA damage, particularly DSB repair, are unclear. In this study, we discovered that CTPS1 is rapidly recruited to DSB sites, indicating that it functions in a rapid DDR that is independent of the long-term effects of pyrimidine deficiency. In addition,

Ser575 phosphorylation of CTPS1 is reported to disrupt its activity⁴⁰, which indicates a possible dynamic regulation of transitioning from recruitment but lower deamidase activity to higher deamidase activity after recruitment of CTPS1.

In conclusion, our data demonstrate that H1(N76D/N77D) is catalysed by CTPS1 in response to DNA damage. Furthermore, H1(N76D/N77D) is a prerequisite for p300 recruitment to Lys75 for acetylation catalysis and decreased nucleosome compaction. Validation of this regulatory model in mouse models and clinical samples showed that CTPS1 is highly correlated with radiotherapy resistance, suggesting that targeting H1 deamidation is a promising strategy for cancer therapy.

Online content

Any methods, additional references, Nature Portfolio reporting summaries, source data, extended data, supplementary information, acknowledgements, peer review information; details of author contributions and competing interests; and statements of data and code availability are available at <https://doi.org/10.1038/s41586-025-08835-0>.

1. Mohan, C., Das, C. & Tyler, J. Histone and chromatin dynamics facilitating DNA repair. *DNA Repair* **107**, 103183 (2021).
2. Song, F. et al. Cryo-EM study of the chromatin fiber reveals a double helix twisted by tetranucleosomal units. *Science* **344**, 376–380 (2014).
3. Fan, Y. et al. Histone H1 depletion in mammals alters global chromatin structure but causes specific changes in gene regulation. *Cell* **123**, 1199–1212 (2005).
4. Bird, A. W. et al. Acetylation of histone H4 by Esa1 is required for DNA double-strand break repair. *Nature* **419**, 411–415 (2002).
5. Chen, C. C. et al. Acetylated lysine 56 on histone H3 drives chromatin assembly after repair and signals for the completion of repair. *Cell* **134**, 231–243 (2008).
6. Zhang, J. et al. PARylated PDHE1 α generates acetyl-CoA for local chromatin acetylation and DNA damage repair. *Nat. Struct. Mol. Biol.* **30**, 1719–1734 (2023).
7. Kusch, T. et al. Acetylation by Tip60 is required for selective histone variant exchange at DNA lesions. *Science* **306**, 2084–2087 (2004).
8. Murr, R. et al. Histone acetylation by Trapp-Tip60 modulates loading of repair proteins and repair of DNA double-strand breaks. *Nat. Cell Biol.* **8**, 91–99 (2006).
9. Smith, R. et al. HPF1-dependent histone ADP-ribosylation triggers chromatin relaxation to promote the recruitment of repair factors at sites of DNA damage. *Nat. Struct. Mol. Biol.* **30**, 678–691 (2023).
10. Guo, Y., Fan, B. & Li, M. PARP molecular functions and applications of PARP inhibitors in cancer treatment. *Genome Instab. Dis.* **4**, 137–153 (2023).
11. Izzo, A. & Schneider, R. The role of linker histone H1 modifications in the regulation of gene expression and chromatin dynamics. *Biochim. Biophys. Acta* **1859**, 486–495 (2016).
12. Vaquero, A. et al. Human SirT1 interacts with histone H1 and promotes formation of facultative heterochromatin. *Mol. Cell* **16**, 93–105 (2004).
13. Geeven, G. et al. Local compartment changes and regulatory landscape alterations in histone H1-depleted cells. *Genome Biol.* **16**, 289 (2015).
14. Brown, D. T., Izard, T. & Misteli, T. Mapping the interaction surface of linker histone H1(0) with the nucleosome of native chromatin in vivo. *Nat. Struct. Mol. Biol.* **13**, 250–255 (2006).
15. Zhou, B. R. et al. Structural insights into the histone H1-nucleosome complex. *Proc. Natl Acad. Sci. USA* **110**, 19390–19395 (2013).
16. Zhou, B. R. et al. Structural mechanisms of nucleosome recognition by linker histones. *Mol. Cell* **59**, 628–638 (2015).
17. Downs, J. A., Kosmidou, E., Morgan, A. & Jackson, S. P. Suppression of homologous recombination by the *Saccharomyces cerevisiae* linker histone. *Mol. Cell* **11**, 1685–1692 (2003).
18. Konishi, A. et al. Involvement of histone H1.2 in apoptosis induced by DNA double-strand breaks. *Cell* **114**, 673–688 (2003).
19. Li, Z. et al. Destabilization of linker histone H1.2 is essential for ATM activation and DNA damage repair. *Cell Res.* **28**, 756–770 (2018).
20. Kamieniarz, K. et al. A dual role of linker histone H1.4 Lys 34 acetylation in transcriptional activation. *Genes Dev.* **26**, 797–802 (2012).
21. Tessarz, P. & Kouzarides, T. Histone core modifications regulating nucleosome structure and dynamics. *Nat. Rev. Mol. Cell Biol.* **15**, 703–708 (2014).
22. Christophorou, M. A. et al. Citrullination regulates pluripotency and histone H1 binding to chromatin. *Nature* **507**, 104–108 (2014).
23. Thorslund, T. et al. Histone H1 couples initiation and amplification of ubiquitin signalling after DNA damage. *Nature* **527**, 389–393 (2015).
24. Kysela, B., Chovanec, M. & Jeggo, P. A. Phosphorylation of linker histones by DNA-dependent protein kinase is required for DNA ligase IV-dependent ligation in the presence of histone H1. *Proc. Natl Acad. Sci. USA* **102**, 1877–1882 (2005).
25. Boudier-Lemosquet, A., Mahler, A., Bobo, C., Dufosse, M. & Priault, M. Introducing protein deamidation: landmark discoveries, societal outreach, and tentative priming workflow to address deamidation. *Methods* **200**, 3–14 (2022).
26. Li, J. et al. Antiviral activity of a purine synthesis enzyme reveals a key role of deamidation in regulating protein nuclear import. *Sci. Adv.* **5**, eaaw7373 (2019).
27. Zhang, J. et al. Species-specific deamidation of cGAS by herpes simplex virus UL37 protein facilitates viral replication. *Cell Host Microbe* **24**, 234–248.e5 (2018).
28. Zhao, J. et al. Deamidation shunts RelA from mediating inflammation to aerobic glycolysis. *Cell Metab.* **31**, 937–955.e7 (2020).

29. Zhao, R. et al. Inhibition of the Bcl-xL deamidation pathway in myeloproliferative disorders. *N. Engl. J. Med.* **359**, 2778–2789 (2008).
30. Deverman, B. E. et al. Bcl-xL deamidation is a critical switch in the regulation of the response to DNA damage. *Cell* **111**, 51–62 (2002).
31. Lynch, E. M. et al. Human CTP synthase filament structure reveals the active enzyme conformation. *Nat. Struct. Mol. Biol.* **24**, 507–514 (2017).
32. Lynch, E. M. et al. Structural basis for isoform-specific inhibition of human CTPS1. *Proc. Natl Acad. Sci. USA* **118**, e2107968118 (2021).
33. Williams, J. C., Kizaki, H., Weber, G. & Morris, H. P. Increased CTP synthetase activity in cancer cells. *Nature* **271**, 71–73 (1978).
34. Ellims, P. H., Gan, T. E. & Medley, G. Cytidine triphosphate synthetase activity in lymphoproliferative disorders. *Cancer Res.* **43**, 1432–1435 (1983).
35. Lin, Y. et al. CTPS1 promotes malignant progression of triple-negative breast cancer with transcriptional activation by YBX1. *J. Transl. Med.* **20**, 17 (2022).
36. Martin, E. et al. CTP synthase 1 deficiency in humans reveals its central role in lymphocyte proliferation. *Nature* **510**, 288–292 (2014).
37. Pfeiffer, C. et al. CTPS1 is a novel therapeutic target in multiple myeloma which synergizes with inhibition of CHEK1, ATR or WEE1. *Leukemia* **38**, 181–192 (2024).
38. Mileskin, L. R. et al. Adjuvant chemotherapy following chemoradiotherapy as primary treatment for locally advanced cervical cancer versus chemoradiotherapy alone (OUTBACK): an international, open-label, randomised, phase 3 trial. *Lancet Oncol.* **24**, 468–482 (2023).
39. Happel, N. & Doenecke, D. Histone H1 and its isoforms: contribution to chromatin structure and function. *Gene* **431**, 1–12 (2009).
40. Rao, Y. et al. Pyrimidine synthesis enzyme CTP synthetase 1 suppresses antiviral interferon induction by deamidating IRF3. *Immunity* **58**, 74–89.e6 (2025).
41. Luijsterburg, M. S. et al. PARP1 links CHD2-mediated chromatin expansion and H3.3 deposition to DNA repair by non-homologous end-joining. *Mol. Cell* **61**, 547–562 (2016).
42. Nosella, M. L. et al. Poly(ADP-ribosylation) enhances nucleosome dynamics and organizes DNA damage repair components within biomolecular condensates. *Mol. Cell* **84**, 429–446.e17 (2024).
43. Fyodorov, D. V., Zhou, B. R., Skoultschi, A. I. & Bai, Y. Emerging roles of linker histones in regulating chromatin structure and function. *Nat. Rev. Mol. Cell Biol.* **19**, 192–206 (2018).
44. Li, Y. et al. Histone H1 acetylation at lysine 85 regulates chromatin condensation and genome stability upon DNA damage. *Nucleic Acids Res.* **46**, 7716–7730 (2018).
45. Gong, F. & Miller, K. M. Mammalian DNA repair: HATs and HDACs make their mark through histone acetylation. *Mutat. Res.* **750**, 23–30 (2013).
46. Jacquet, K. et al. The TIP60 complex regulates bivalent chromatin recognition by 53BP1 through direct H4K20me binding and H2AK15 acetylation. *Mol. Cell* **62**, 409–421 (2016).
47. Cheung, P. et al. Synergistic coupling of histone H3 phosphorylation and acetylation in response to epidermal growth factor stimulation. *Mol. Cell* **5**, 905–915 (2000).
48. Lo, W. S. et al. Phosphorylation of serine 10 in histone H3 is functionally linked in vitro and in vivo to Gcn5-mediated acetylation at lysine 14. *Mol. Cell* **5**, 917–926 (2000).
49. Lee, J. S., Smith, E. & Shilatifard, A. The language of histone crosstalk. *Cell* **142**, 682–685 (2010).
50. Taverna, S. D. et al. Yng1 PHD finger binding to H3 trimethylated at K4 promotes NuA3 HAT activity at K14 of H3 and transcription at a subset of targeted ORFs. *Mol. Cell* **24**, 785–796 (2006).
51. Robinson, N. E. & Robinson, A. B. Prediction of protein deamidation rates from primary and three-dimensional structure. *Proc. Natl Acad. Sci. USA* **98**, 4367–4372 (2001).
52. Robinson, N. E. et al. Structure-dependent nonenzymatic deamidation of glutamyl and asparagyl pentapeptides. *J. Pept. Res.* **63**, 426–436 (2004).
53. Robinson, A. B., McKerrow, J. H. & Legaz, M. Sequence dependent deamidation rates for model peptides of cytochrome C. *Int. J. Pept. Protein Res.* **6**, 31–35 (1974).
54. Zhao, J., Li, J., Xu, S. & Feng, P. Emerging roles of protein deamidation in innate immune signaling. *J. Virol.* **90**, 4262–4268 (2016).
55. Cui, J. et al. Glutamine deamidation and dysfunction of ubiquitin/NEDD8 induced by a bacterial effector family. *Science* **329**, 1215–1218 (2010).
56. Sanada, T. et al. The *Shigella flexneri* effector OspI deamidates UBC13 to dampen the inflammatory response. *Nature* **483**, 623–626 (2012).
57. Flatau, G. et al. Toxin-induced activation of the G protein p21 Rho by deamidation of glutamine. *Nature* **387**, 729–733 (1997).
58. Schmidt, G. et al. Gln 63 of Rho is deamidated by *Escherichia coli* cytotoxic necrotizing factor-1. *Nature* **387**, 725–729 (1997).
59. Shukla, S. K. et al. MUC1 and HIF-1 α signaling crosstalk induces anabolic glucose metabolism to impart gemcitabine resistance to pancreatic cancer. *Cancer Cell* **32**, 71–87.e7 (2017).
60. Sun, Z., Zhang, Z., Wang, Q. Q. & Liu, J. L. Combined inactivation of CTPS1 and ATR is synthetically lethal to MYC-overexpressing cancer cells. *Cancer Res.* **82**, 1013–1024 (2022).

Publisher's note Springer Nature remains neutral with regard to jurisdictional claims in published maps and institutional affiliations.



Open Access This article is licensed under a Creative Commons Attribution-NonCommercial-NoDerivatives 4.0 International License, which permits any non-commercial use, sharing, distribution and reproduction in any medium or format, as long as you give appropriate credit to the original author(s) and the source, provide a link to the Creative Commons licence, and indicate if you modified the licensed material. You do not have permission under this licence to share adapted material derived from this article or parts of it. The images or other third party material in this article are included in the article's Creative Commons licence, unless indicated otherwise in a credit line to the material. If material is not included in the article's Creative Commons licence and your intended use is not permitted by statutory regulation or exceeds the permitted use, you will need to obtain permission directly from the copyright holder. To view a copy of this licence, visit <http://creativecommons.org/licenses/by-nc-nd/4.0/>.

© The Author(s) 2025

Methods

Cell culture

HeLa, HCT116, A549, H1975, HepG2, Hepa1-6, NCI-H1299, HCC1937, MCF7, T47D-KBluc, 786-O, A-498, 5637, T24 and HEK293T cells were obtained from the American Type Culture Collection. AsiSI-ER-U2OS-AID cells were provided by G. Legube; PARP1-KO, EJ5-U2OS and DR-U2OS cells were provided by X. Xu; and U2OS-265 reporter cells were provided by R. Greenberg. All cells were cultured in Dulbecco's modified Eagle medium (DMEM) supplemented with 10% fetal bovine serum (FBS) and 1% penicillin–streptomycin, and maintained in a humidified incubator at 37 °C under 5% CO₂ and were free of mycoplasma contamination.

Plasmid construction and transfection

H1.4 (also known as *H1-4*) and *CTPS1* cDNAs were cloned from HeLa cells and subcloned separately into p3×Flag-CMV10, EGFP-C1, pET28b and pGEX-4T3 vectors. The cDNAs for *p300* (also known as *EP300*), *CBP* (*CREBBP*), *hMOF* (*KAT8*), *TIP60* (*KAT5*) and *PCAF* (*KAT2B*) were cloned into p3×Flag-CMV-10. The cDNAs for p300 HAT were cloned into p3×Flag-CMV-10, mCherry-N1, EGFP-C1 and pGEX-6P1 vectors. The cDNA for p300 fragments were cloned into pGEX-6P1. The cDNAs for H1.1, H1.2, H1.3 and H1.5 were cloned into p3×Flag-CMV-10. All mutant constructs were generated using the wild-type construct as a template with a Mut Express II Fast Mutagenesis Kit (Vazyme Biotech) according to the manufacturer's protocols. A list of the primers for plasmid construction is provided in Supplementary Table 1.

For transient transfections, cells were transfected with the above mentioned plasmids using UltraFection 3.0 reagent (4A Biotech), following the manufacturer's instructions. Cells were also transfected with either non-targeting control or gene-specific siRNAs using INTERFERin transfection reagent (Invitrogen), according to the manufacturer's guidelines. All siRNA sequences are listed in Supplementary Table 2. Homozygous insertions and knock-ins were confirmed by Sanger sequencing and western blotting. A list of the oligos and sequences for the single guide RNAs (sgRNAs) is provided in Supplementary Table 3.

Stable cell line establishment

For knockout cell lines, pLentivirus2 plasmids carrying CRISPR–Cas9 and an sgRNA targeting H1.1–H1.4 or *CTPS1* were transfected into HEK293T cells for 72 h using polyethylenimine (Polysciences) according to the manufacturer's instructions. The culture medium containing the lentivirus was collected and transferred to HeLa cells in the presence of 8 µg ml⁻¹ polybrene. After infection for 48 h, cells were sub-seeded into 96-well plates and selected for single colonies using puromycin (2 µg ml⁻¹) for 1 week. Proteins were extracted from WCLs of surviving colonies for western blot analysis.

For overexpressing cell lines, the pCDH-CMV-MCS-EF1 lentivirus carrying sgRNA-resistant mutated Flag–H1.4 was transfected into H1.4-KO cells for 48 h. The lentivirus carrying sgRNA-resistant Flag–CTPS1-WT or ED was transfected into CTPS1-KO cells for 48 h. The transfected cells were then cultured in medium containing puromycin (5 µg ml⁻¹) for 10 days. After antibiotic selection, cells were sub-seeded into 96-well plates for selecting single colonies. Proteins were extracted from WCLs of surviving colonies for western blot analysis.

Knock-in cell line establishment

An FKBP12 degron tag-mediated system to deplete CTPS1 (FKBP–CTPS1) in HeLa cells was established as previously described⁶¹. To generate the endogenous dTAG-inducible degradation system for CTPS1, sgRNA targeting the start codon region and pUC19 plasmid were co-transfected into the HeLa cells or H1.4-KO HeLa cells expressing wild-type or mutant Flag–H1.4. The pUC19 plasmid contained the following elements: left and right homology arms, as well as FKBP12(F36V), 3×Flag tags, P2A and a gene encoding blasticidin-S deaminase (BSD). The transfected cells were selected with 10 µg ml⁻¹ blasticidin-S-selective antibiotic

(blasticidin-S HCl; A1113903, Thermo Fisher Scientific), and sub-seeded into 96-well plates for selecting single colonies and screened for correct biallelic integration. All homozygous insertions and knock-ins were confirmed by PCR and western blotting.

Subcellular fractionation

For histone acid extraction, cell pellets were lysed on ice in hypotonic buffer containing 0.4 M sulfuric acid and precipitated with trichloroacetic acid at 4 °C overnight. The histone pellet was washed twice with ice-cold acetone and then air-dried. The pellet was then resuspended in an equal volume of ddH₂O and 2× loading buffer and boiled for 5 min before immunoblotting.

For chromatin fractionation, cells were harvested and lysed on ice in buffer I (50 mM HEPES pH 7.5, 150 mM NaCl and 1 mM EDTA) containing 0.1% Triton X-100 and 1% protease inhibitor cocktail for 3 min. After centrifugation (13,000g for 3 min), the supernatant was discarded, and the pellet was resuspended on ice in buffer I containing 200 µg ml⁻¹ RNaseA and 1% protease inhibitor cocktail for 3 min. After a second centrifugation, the pellet was resuspended in an equal volume of PBS and 2× loading buffer and boiled for 5 min before immunoblotting.

For WCL extraction, cells were harvested and lysed on ice for 30 min in lysis buffer (20 mM Tris-HCl pH 7.5, 137 mM NaCl, 10% glycerol, 1% NP-40, 2 mM EDTA and 1% protease inhibitor cocktail), followed by centrifugation at 13,000g at 4 °C for 15 min. After centrifugation, the pellet was resuspended in 5× loading buffer and boiled for 5 min before immunoblotting.

Co-immunoprecipitation

For endogenous co-immunoprecipitation, WCLs were prepared on ice for 30 min in lysis buffer (20 mM Tris-HCl pH 7.5, 137 mM NaCl, 10% glycerol, 1% NP-40, 2 mM EDTA and 1% protease inhibitor cocktail), followed by centrifugation at 13,000g at 4 °C for 15 min. The lysates were immunoprecipitated with the indicated antibodies (2 µg) overnight at 4 °C, followed by the addition of 30 µl protein G or protein A agarose gel beads. After incubation for a further 2 h at 4 °C, the beads were washed three times in NP-40 buffer (20 mM Tris-HCl pH 8.0, 137 mM NaCl, 1% NP-40, 10% glycerol, 2 mM EDTA and 1% protease inhibitor cocktail) and centrifuged at 100g at 4 °C for 1 min. The precipitated components were boiled and analysed by western blotting.

For Flag co-immunoprecipitation, WCLs were extracted and immunoprecipitated with Flag–agarose gel beads overnight at 4 °C. The beads were washed three times in NP-40 buffer and centrifuged at 100g at 4 °C for 1 min. The immunoprecipitated proteins were eluted overnight at 4 °C with 50 µl 3× Flag peptide (Sigma-Aldrich; 0.125 mg ml⁻¹) in TBS buffer (50 mM Tris-HCl, pH 7.4, and 150 mM NaCl). The supernatant was boiled with 2× SDS loading buffer (100 mM Tris-HCl pH 6.8, 4% SDS, 20% glycerol, 0.2% bromophenol blue and 2% β-mercaptoethanol) for western blotting.

Protein purification and GST pull-down

His-tagged or GST-tagged plasmids were transformed into *E. coli* BL21 cells and induced with 0.1 mM isopropyl β-D-1-thiogalactopyranoside (IPTG) overnight at 16 °C, followed by purification using an Ni-IDA Sepharose gel or glutathione–Sepharose 4B beads, respectively. Equal amounts of individual His-fusion proteins were incubated for 4 h at 4 °C with GST-fusion proteins in TEN buffer (10 mM Tris-HCl pH 8.0, 1 mM EDTA and 100 mM NaCl). The beads were then washed three times in TEN buffer with centrifugation at 100g at 4 °C for 1 min and boiled for 5 min in an equal volume of 2× SDS loading buffer before immunoblotting or Coomassie brilliant blue staining.

Western blot analysis

Equivalent amounts of boiled protein samples were separated by SDS–PAGE (6–15% gels) and transferred to nitrocellulose membranes. After blocking with 5% BSA, the membranes were incubated overnight at

4 °C with the indicated primary antibodies and then with horseradish peroxidase (HRP)-conjugated secondary antibodies for 2 h at room temperature. The proteins were detected using an ECL kit (WBULS0500, Millipore-Sigma Aldrich) and visualized with a Tanon 5200SF Imaging System. A list of information on antibodies is provided in Supplementary Table 4.

Mass spectrometry

For H1 PTM identification, histones were separated by SDS-PAGE and stained with Coomassie brilliant blue. The bands were then sent to Win-innovate Bio for liquid chromatography-tandem mass spectrometry to identify H1 PTMs. The desired PAGE bands were destained, dehydrated and digested in the gel in mass spectrometry-grade trypsin (V5280, Promega Biotech) for 12 h at 37 °C. Peptides were extracted from the gels with 70% acetonitrile/water containing 0.5% trifluoroacetic acid, then lyophilized and resuspended in 5% acetonitrile/water (0.1% formic acid), before 6 µl of the peptide mixture was loaded onto a nanoViper C18 (Acclaim PepMap 100, 75 µm × 2 cm) trap column. The peptides were chromatographically separated on an Easy nLC 1200 system (Thermo Fisher). Tandem mass spectra were acquired on a Q Exactive mass spectrometer (Thermo Fisher) equipped with a Nano Flex ion source. The tandem mass spectrometry raw data were processed for protein identification and PTM analysis using PEAKS Studio 8.5 (Bioinformatics Solutions). The database search parameters were set as follows: proteome database of Uniprot-human including 20,603 protein entries or target protein of H1.2_HUMAN Histone (Uniprot accession number: P16403); mass tolerance for precursor and fragment ions at 10 ppm and 0.05 Da, respectively; variable modifications of acetylation (protein-N terminus, K), oxidation (M), deamidation (NQ) and fixed modification of carbamidomethylation (C). Label-free quantification analysis of PTMs between different samples was performed based on the peptide area in each sample, calculated by distributing the associated peptide feature area, including different *m/z*-extracted ion chromatograph areas.

For CTPS1 phosphorylation site identification, WCLs were extracted, immunoprecipitated using anti-Flag, and separated by SDS-PAGE and stained with Coomassie brilliant blue. The bands were then sent to PTM Bio for liquid chromatography-tandem mass spectrometry to identify CTPS1 phosphorylation sites.

Two-dimensional gel electrophoresis

The extracted histone proteins were dissolved in 150 µl rehydration buffer (8 M urea, 2% CHAPS, 0.5% IPG buffer and 0.002% bromophenol blue), and then loaded onto isoelectric focusing (IEF) strips using the following programme: 20 V for 10 h (rehydration); 500 V for 1 h; 1,000 V for 1 h; 1,000–5,000 V for 4 h; and 5,000 V for 4 h. Following IEF, the strips were incubated for 15 min in SDS equilibration solution containing 10 mg ml⁻¹ dithiothreitol (DTT) and then for another 15 min in SDS equilibration buffer (50 mM Tris-HCl pH 8.8, 6 M urea, 30% glycerol, 2% SDS and 0.001% bromophenol blue) containing 2-iodoacetamide. Strips were washed in SDS-PAGE buffer and resolved by SDS-PAGE before immunoblotting.

CUT&Tag-seq and ATAC-seq

U2OS-AsiSI-ER-AID cells were exposed to 500 nM 4OHT for 4 h. CUT&Tag or ATAC-seq was performed using the Hyperactive Universal CUT&Tag Assay Kit or Hyperactive ATAC-Seq Kit (Vazyme).

CUT&Tag was performed with anti-H1(N76D/N77D), anti-H1K75ac, anti-H1K75ac2ND or anti-CTPS1 antibodies. In brief, nuclei from 1 × 10⁵ cells were extracted with the provided nuclei extraction buffer and then incubated with 10 µl ConA beads. Then, 1 µg anti-H1(N76D/N77D), anti-H1K75ac, anti-H1K75ac2ND or anti-CTPS1 antibodies was added and cultured for 2 h at room temperature. After washing twice with the provided dig-wash buffer, 0.5 µg secondary antibody was added and incubated at room temperature for 30 min. After washing twice with

dig-wash buffer, 2 µl pA/G-Tn5 was cultured with the beads for 1 h, followed by tagmentation at 37 °C for 1 h. The reaction was stopped with proteinase K and buffer B/L, and DNA was extracted with DNA extraction beads for subsequent PCR to amplify the libraries.

For ATAC-seq, 5 × 10⁴ cells were harvested and resuspended in the lysis buffer (10 mM Tris-HCl pH 7.5, 10 mM NaCl, 3 mM MgCl₂ and 0.05% NP-40). The lysates were centrifuged for 3 min at 500g at 4 °C. The cell pellet was resuspended in transposition reaction mix and incubated at 37 °C for 45 min. The transposed DNA was purified using ATAC DNA extraction beads before PCR to amplify the libraries. The amplified ATAC-seq library was purified with ATAC DNA Clean Beads and eluted with 30 µl ddH₂O.

Libraries were created using the TruePrep Index Kit (Vazyme) and sent to Novogene for sequencing on an Illumina NovaSeq 6000 platform. The raw reads were processed using Fastp (v0.23.4) to eliminate adaptors and low-quality sequences. Bowtie2 (v2.5.4) was applied for alignment to the hg38 human genome reference, using the parameters ‘-very-sensitive-no-mixed-no-discordant’. Samtools was used to convert SAM files to BAM format, applying a filter criterion of a minimum mapping quality score of 10. Duplicate reads were removed using the Picard tool. The bamCoverage function was then used to transform BAM files into BW format, with normalization applied using the parameter ‘-normalizeUsing BPM’. The top 80 BLESS signal enzyme-cutting sites⁶² were subjected to coordinate conversion from hg19 to hg38 using the liftOver utility. The generation of metagene profiles and heatmaps, which display the signals of each histone modification and open chromatin at DSBs, was accomplished using the computeMatrix and plotHeatmap functions of deepTools (v3.5.5). DSB sites were classified as prone to homologous recombination or NHEJ according to previous research⁶².

Comet assay

Cells were exposed to 10 Gy IR or 20 µM VP16 for 2 h. After release for the indicated time, cells were resuspended at a density of 5 × 10⁵ per millilitre in ice-cold PBS and combined with molten low-melting-point agarose at a 1:10 (vol/vol) ratio. The cell-agarose mixture was spread onto pre-warmed comet slides and kept at 4 °C until the agarose solidified. The slides were then immersed in lysis buffer (2.5 M NaCl, 100 mM EDTA, 10 mM Tris-HCl and 1% Triton X-100) overnight at 4 °C. The slides were incubated in freshly prepared running buffer (1 mM Na₂EDTA and 300 mM NaOH) for 30 min, followed by electrophoresis in running buffer at 1.0 V cm⁻¹ for 30 min. Slides were washed twice in 75% ethanol for 5 min and dried at 37 °C. Cells were then stained with 5 µg ml⁻¹ propidium iodide for 30 min in the dark before images were captured using an Olympus BX51 fluorescent microscope. Comet tail moments were measured using the OpenComet plugin in ImageJ; 50 nuclei or 5 fields were captured and counted.

Enzyme-linked immunosorbent assay

The specificities of antibodies targeting H1(N76D/N77D), H1K75ac and H1 with spontaneous modifications of three sites (H1K75ac2ND) were validated by ELISA. The purified antibodies were incubated in 96-well plates precoated with 50 ng of modified or negative control peptides. The wells were then washed three times with PBS, and the absorbance of each well was measured at 450 nm using a microtitre plate reader.

Microscale thermophoresis

A total of 10 µl of 2 µM His-H1.4 or His-H1.4-KQ proteins purified from *E. coli* was mixed with 10 µl PBST binding buffer (PBS containing 0.05% Tween). After thorough mixing, 10 µl of the mixture was removed and serially diluted twofold. This dilution procedure was repeated 16 times as ligands. A total of 10 µl of 2 nM DNA-Cy5 were mixed with each ligand and then a Monolith NT.115 (NanoTemper Technologies) standard capillary was inserted into each mixture. The MST device was started after placing the capillaries in locations 1 through 16 in the sample tray.

Article

The data were analysed by plotting peptide concentrations against liquid-induced fluorescence changes (change in raw fluorescence on the y axis). Curve fitting was performed by using MO. Affinity analysis and the given K_d values were calculated with 95% confidence levels.

Immunofluorescent staining

Wild-type and CTPS1-KO HeLa cells, or H1.4-KO HeLa cell lines stably expressing mutant H1.4 (5×10^4) were seeded into a 35-mm glass-bottomed dish and cultured in a humidified incubator at 37 °C under 5% CO₂ for 48 h. Cells were treated with 10 Gy IR or 20 μ M VP16 for 2 h, and then fixed at indicated time with 1 ml of 4% tissue fixation solution at 4 °C for at least 30 min, washed three times with PBS, and then permeabilized with pre-cooled methanol at –20 °C for 30 min. After blocking with 5% BSA for 1 h at room temperature, the cells were washed and incubated overnight at 4 °C with the indicated antibodies. After washing three times with PBS, the cells were incubated with secondary antibodies conjugated to Alexa Fluor 488 or 594 for 1 h at room temperature. After washing three times with PBST, DAPI was used to stain nuclear DNA. Immunofluorescent images were captured under a Nikon confocal microscope.

In vitro acetylation assay

GST–p300 HAT was purified and incubated with substrates in acetylation buffer (50 mM Tris-HCl pH 8.0, 50 mM NaCl, 4 mM MgCl₂, 0.1 mM EDTA, 1 mM DTT and 10% glycerol) with or without acetyl-CoA (5 mM), for 1 h at 30 °C. The reactions were stopped by adding 5 \times protein sample buffer (250 mM Tris-HCl pH 6.8, 10% SDS, 50% glycerol, 0.5% bromophenol blue and 5% β -mercaptoethanol), and the samples were boiled for 5 min before separation by SDS–PAGE and immunoblotting.

In vitro deamidation assay

Flag–CTPS1 was purified from transfected HEK293T cells, and His–H1.4 or GST–H1.4 was purified from *E. coli* cells. Flag–CTPS1 (8 μ M) was incubated at 21 °C for 3 min in reaction buffer containing 20 mM Tris-HCl (pH 7.9) and 10 mM MgCl₂. Flag–CTPS1 was then combined with pre-warmed (37 °C) nucleotides at final concentrations of 2 mM UTP, 2 mM ATP and 0.2 mM GTP for 30 min. The substrate His–H1.4 (2 μ M) was added and incubated at 37 °C for an additional 45 min to allow for polymerization. The samples were then subjected to 2DGE and immunoblotting.

Laser micro-irradiation-coupled live-cell imaging

HeLa or HCT116 cells (7×10^4) were seeded into a 35-mm glass-bottomed dish and transfected with mCherry–p300 HAT, GFP–CTPS1 or GFP–PARP1 for 48 h. The cells were locally irradiated with a 365-nm pulsed nitrogen UV laser (16 Hz pulse, 41% laser output) generated from a MicroPoint system (Andor). This system was coupled directly to the epifluorescence path of the Nikon A1 confocal imaging system, and timelapse images were captured every 10 s for the indicated time. The intensity of the irradiation path signal from indicated cells was calculated using ImageJ software.

Laser micro-irradiation-coupled immunofluorescence

Wild-type or CTPS1-KO HeLa cells (3×10^5) were seeded into a 35-mm glass-bottomed dish and locally irradiated with a 365-nm pulsed nitrogen UV laser (16 Hz pulse, 41% laser output) generated from a MicroPoint system (Andor). Cells were fixed at 5 min post-irradiation with 1 ml of 4% tissue fixation solution at 4 °C for at least 30 min, washed three times with PBS, and then permeabilized with pre-cooled methanol at –20 °C for 30 min. After blocking with 5% BSA for 1 h at room temperature, the cells were washed and co-incubated overnight at 4 °C with anti-H1(N76D/N77D), anti-H1K75ac, anti-H1K75ac2ND or anti-CTPS1 and anti- γ H2AX antibodies. After washing three times with PBS, the cells were incubated with secondary antibodies conjugated to Alexa Fluor 488 or 594 for 1 h at room temperature in the dark. After

washing three times with PBST, DAPI was used to stain the nuclear DNA. Immunofluorescent images were captured under a Nikon confocal microscope.

RT–qPCR assay

Total RNA was extracted from cells using TRIzol reagent. The suspension was centrifuged (13,000g for 5 min), and the upper layer was precipitated using isopropanol and centrifuged at 13,000g for 10 min at 4 °C. After washing with 75% ethanol, the RNA was treated with DNase I for 30 min at 37 °C to remove contaminating DNA, and then reverse transcribed into cDNA using a QuantScript RT Kit (Tiangen) according to the manufacturer's instructions.

ChIP–qPCR

U2OS-AsiSI-ER-AID cells (1.5×10^7) on 150-mm cell culture dishes were crosslinked using 1% formaldehyde for 10 min and quenched with 125 mM glycine for 2 min at room temperature. The cells were collected, washed twice with cold PBS and resuspended in immunoprecipitation buffer (150 mM NaCl, 50 mM Tris-HCl pH 7.5, 5 mM EDTA, 0.5% NP-40 and 1% Triton X-100) for ultrasound fragmentation. After centrifugation at 12,000g for 10 min at 4 °C, the supernatant was incubated with 1 μ g normal rabbit IgG or anti-H1(N76D/N77D) antibody immobilized on protein A/G Sepharose beads. The beads were washed five times with immunoprecipitation buffer and mixed with 100 μ l of 10% Chelex (Bio-Rad). The samples were boiled for 10 min and the supernatants were collected. The pellets were resuspended in 120 μ l of ddH₂O and centrifuged at 10,000g for 1 min at 4 °C. The supernatants were combined as the IP DNA pool. The immunoprecipitation DNA pool and 2% input DNA were used as templates for qPCR analysis using SYBR Green Supermix (Vazyme) on a qTOWER3G Touch Real-Time PCR Detection System (Analytik Jena). All samples were analysed in triplicate.

ChIP–re-ChIP

U2OS-AsiSI-ER-AID cells (5×10^7) on 150-mm cell culture dishes were crosslinked using 1% formaldehyde for 10 min and quenched with 125 mM glycine for 2 min at room temperature. The cells were collected, washed twice with cold PBS and resuspended in IP buffer (150 mM NaCl, 50 mM Tris-HCl pH 7.5, 5 mM EDTA, 0.5% NP-40 and 1% Triton X-100) for ultrasound fragmentation. After centrifugation at 12,000g for 10 min at 4 °C, the supernatant was collected for the ChIP–re-ChIP assay using the Re-ChIP-IT kit (S3016, Active Motif); 1% of the input DNA was stored as a control. In brief, chromatin was incubated with 3 μ g H1.4 antibody or normal rabbit IgG and 25 μ l protein G beads overnight at 4 °C. The beads were washed twice with both ChIP buffer 1 and ChIP buffer 2. The first ChIP reaction was eluted with 100 μ l Re-ChIP-IT Elution buffer for 30 min at room temperature. The first ChIP chromatin was then collected with desalting columns and subjected to the second ChIP (containing 25 μ l LSV protein G beads, 3 μ g anti-H1(N76D/N77D), anti-H1K75ac or anti-H1K75ac-2ND antibodies or normal rabbit IgG) overnight at 4 °C. The beads were washed twice with both ChIP buffer 1 and ChIP buffer 2, and eluted with elution buffer AM2 for 15 min at room temperature. The chromatin was then reversed crosslinked and treated with proteinase K. The ChIP–re-ChIP DNA and input DNA were used as templates for qPCR analysis using SYBR Green Supermix (Vazyme) on a qTOWER3G Touch Real-Time PCR Detection System (Analytik Jena). All samples were analysed in triplicate.

In situ DSB reporter assay

265-U2OS cells (7×10^4) were seeded into a 35-mm glass-bottomed dish. The cells were transfected with GFP vector, GFP–p300 HAT or GFP–CTPS1 for 48 h before exposure to 4OHT (500 nM) and shield I (30 ng ml^{-1}) for 6 h. The cells were then incubated with 1 ml of 4% tissue fixation solution at 4 °C for at least 30 min and washed three times with PBS. DAPI was used to stain nuclear DNA. Immunofluorescent images were captured under a Nikon confocal microscope.

Homologous recombination and NHEJ reporter assays

pDR-GFP-U2OS (homologous recombination) or pEJ5-GFP-U2OS (NHEJ) cells (7×10^4) were seeded into a 60-mm cell culture dish. The cells were transfected with CTPS1, p300 or control siRNA for 12 h, followed by transfection with Flag-tagged wild-type H1.4 or 2ND/2NR/2NA/KQ/KR mutants for an additional 12 h. The cells were then infected with a retrovirus expressing I-SceI for a further 48 h. After trypsinization, the cells were collected for flow cytometric analysis.

In situ proximity ligation assay

H1.4-KO HeLa cells (7×10^4) were seeded into a 35-mm glass-bottomed dish. The cells were exposed, or not, to 10 Gy IR, then incubated with 1 ml of 4% tissue fixation solution at 4 °C for at least 30 min. The cells were washed three times with PBS, followed by permeabilization with pre-cooled methanol at -20 °C for 30 min. After washing and blocking with 5% BSA for 1 h at room temperature, the cells were double-stained for PLA with anti-p300 and anti-H1.4 or anti-CTPS1 and anti-Flag using the Duolink In Situ Red Starter Kit (Sigma). Images were captured under a Nikon confocal microscope, and PLA foci were automatically quantified using ImageJ software.

MNase assay

MNase assays were performed as previously described⁶³. In brief, HeLa cells (7×10^6) were treated with VP16 (40 μ M) for 1 h. After centrifugation (1,500g for 5 min), the cell pellets were resuspended in buffer A (10 mM HEPES pH 7.9, 10 mM KCl, 1.5 mM MgCl₂, 0.34 M sucrose, 10% glycerol, 1 mM DTT, 0.1% Triton X-100 and protease inhibitor cocktail). After incubation on ice for 8 min, the lysates were centrifuged at 13,000g for 3 min at 4 °C. The pellet was further lysed in buffer B (3 mM EDTA, 0.2 mM EGTA, 1 mM DTT and protease inhibitor cocktail) for 30 min on ice, followed by centrifugation at 1,700g for 5 min. The pellet was resuspended in MNase buffer (200 mM Tris-HCl pH 8.0, 50 mM NaCl and 25 mM CaCl₂) with 10 U MNase for 1 min at 25 °C, and the reaction was stopped by adding 0.5 M EDTA. After incubation on ice for 10 min, RNase A and proteinase K were added. The DNA was separated by 1.2% agarose gel electrophoresis and the intensity of each lane was analysed using ImageJ.

Nucleosome stability assay

HeLa cells (7×10^6) were treated with VP16 (40 μ M) for 1 h and then collected and resuspended in 500 μ l buffer A (20 mM HEPES pH 7.9, 0.5 mM DTT, 1 mM PMSF, 1.5 mM MgCl₂, and 0.1% Triton) containing either 1 M or the indicated concentrations of NaCl. Samples were then ultracentrifuged at 100,000g (Ultracentrifuge, Beckman Coulter) for 20 min, and the supernatant containing the released histones was collected for further analysis.

Chromosome aberration assay

Chromosome metaphase spreading assays were performed to investigate chromosomal abnormalities. The cells were exposed to 3 Gy IR and collected after 2 h of recovery and 8 h of pretreatment with colchicine (0.4 μ g ml⁻¹). After exposure to a hypotonic solution containing 56 mM KCl, the cells were preserved in a 3:1 methanol:acetic acid (v/v) solution. The cells were then dropped onto alcohol-cleaned slides and stained with Giemsa. Images were obtained using a DragonFly confocal imaging system (Andor); more than 100 mitotic chromosomes were randomly selected and examined in each experiment.

Colony formation assay

After 1 h of IR or VP16 treatment, equivalent numbers of cells (control group $n = 500$; experimental group $n = 5,000$) were seeded into 60-mm cell culture dishes and cultured for 2 weeks at 37 °C under 5% CO₂. The cells were then stained with 1 \times crystal violet, and colonies containing more than 50 cells were counted.

Molecular docking

The AlphaFold Protein Structure Database (<https://alphafold.ebi.ac.uk/>) was used to predict the potential structure of CTPS1 (UniProt P17812). Histone H1.4 or H1.4-2ND were predicted by AlphaFold 2 (<https://colab.research.google.com/AlphaFold2.ipynb>).

The structure of p300 HAT was obtained from a previous report⁶⁴ (<https://www.rcsb.org>). GRAMM (<https://gramm.compbio.ku.edu>) and PyMol were used for virtual verification of the binding pocket and hotspot amino acids of H1.4 with CTPS1, and H1.4 or H1.4-2ND with the p300 HAT. The structures of the binding between H1.4 and linker DNA were obtained from a previous report⁶⁵ (<https://www.rcsb.org>). The Lys75, Asn76 and Asn77 amino acids were mutated by PyMol based on the reported wild-type structure. The binding between H1.4 or H1.4-QDD to linker DNA were visualized by PyMol.

Xenograft tumour model

Wild-type or CTPS1-KO HeLa cells, or H1.4-mutant HeLa cell lines with stable expression of Flag-H1.4-RRR or Flag-H1.4-RAA, were trypsinized, counted and resuspended at a 2:1 (v/v) ratio in PBS:Matrigel. The cells (5×10^6 in 100 μ l of the mixture) were then seeded subcutaneously into 4-week-old female BALB/c nude mice (WuXi AppTec). The mice were randomly divided into IR therapy and control groups (six mice per group). For the therapy group, the tumour site was exposed to 3 Gy IR every 3 days, and the tumour size was measured after each treatment. Tumour volumes were assessed on the indicated days using Vernier calipers and calculated using the formula: volume = $0.5 \times l \times \text{width}^2$. Mice were euthanized (via cervical dislocation) after three or four treatments, and the tumours were weighed and stored in liquid nitrogen or fixed in formalin. The samples were thawed from liquid nitrogen, and WCLs or histones were isolated as described above. The protein samples were analysed by western blotting using the indicated antibodies. The use of animals in this study was approved by the Institutional Animal Care and Use Committee (The mechanisms of chromatin remodeling during early stage of DNA damage response, 202400110) of Shenzhen University.

Immunohistochemistry

Sections (5 μ m) from formalin-fixed, paraffin-embedded archival tissues were deparaffinized, rehydrated and rinsed in distilled water. Antigen retrieval was achieved by incubating the slides with 1 mM EDTA buffer (pH 8.0) for 10 min in a pressure cooker. Endogenous peroxidase activity was blocked by incubating the slides in 3% hydrogen peroxide in methanol for 30 min. The sections were then stained for 16 h at 4 °C with polyclonal antibodies to CTPS1 and Ki-67 (1:100 and 1:500, respectively), and chromogen development was performed using the universal HRP Multimer UltraView Kit on a Benchmark XL (Ventana Medical Systems). Formalin-fixed, paraffin-embedded tissue sections were stained using a TUNEL Apoptosis Detection Kit (Yeasen) according to the manufacturer's instructions. CTPS1 expression levels in tissue microarrays were evaluated using ImageJ software by considering the staining intensity and region.

Clinical patient samples

A total of 33 paired human cervical tumour and para-tumour samples were obtained from clinical patients diagnosed and treated with radiotherapies at Shanghai First Maternity and Infant Hospital. The samples were thawed from liquid nitrogen. WCLs were isolated using RIPA lysis buffer, and histone proteins were extracted in H₂SO₄. The protein samples were then analysed by western blotting using the indicated antibodies. A tissue microarray chip consisting of 58 cervical cancer samples from patients before radiotherapy was provided by Fudan University Shanghai Cancer Center. CTPS1 expression levels were determined by immunohistochemistry. All studies using human specimens were approved by the Clinical Research Ethics Committee of

Shenzhen University. The patients provided written informed consent for the use of their resected tissues for research purposes. Data used for survival analyses in gastric and lung cancers were obtained from the KM Plotter website (<https://www.kmplot.com/analysis/>).

Antibody development

The anti-H1(N76D/N77D), anti-H1K75ac and anti-H1K75ac2ND antibodies were developed by PTM Bio. In brief, antigenic polypeptides were designed and synthesized for animal immunization (CYDVEK-DDSRIK for anti-H1(N76D/N77D); CAGYDVE-(acetyl)K-NNSRIK for anti-H1K75ac; AGYDVE-(acetyl)K-DDSRIK for anti-H1K75ac2ND, immunization peptide). An unmodified control polypeptide was designed and synthesized for purification and detection purposes (CYDVEKNNSRIK for anti-H1(N76D/N77D); CAGYDVEKNNSRIK for anti-H1K75ac; AGYDVE-(acetyl)K-NNSRIK and AGYDVEKDDSRIK for anti-H1K75ac2ND). The polypeptides were conjugated with KLH for rabbit immunization. The immunogen was diluted with physiological saline and then mixed 1:1 with the corresponding adjuvant. The antigen and adjuvant were completely mixed to form a stable emulsion and then injected into six healthy New Zealand rabbits. Each rabbit was immunized four times. On the forty-fifth day, 30 ml of whole blood was collected and centrifuged. After centrifugation, the supernatant was collected for serum screening by ELISA and Dot blot. Positive serum samples were purified. Protein A column was packed and equilibrated with 10 volumes of pre-cooled PBS buffer solution. The filtered sample was loaded onto the equilibrated protein A column. The column was washed with PBS buffer and eluted with 150 mM glycine buffer. The crude IgG obtained from protein A purification was loaded onto the equilibrated antigen polypeptide affinity chromatography column to specifically enrich the target antibody. The target antibody obtained in the previous step was loaded onto an unmodified affinity chromatography column to remove nonspecific antibody components. The effluent was directly collected.

Statistics and reproducibility

GraphPad Prism 9.0.0 was used for data analysis. Each group of data was subjected to Kolmogorov–Smirnov tests, Anderson–Darling tests, D’Agostino–Pearson omnibus tests or Shapiro–Wilk tests for normal distribution when applicable. Student’s unpaired two-tailed *t*-tests were used to determine the significance between two selected groups of normally distributed data, unless indicated in the figure legends. $P < 0.05$ was considered statistically significant. For damaged versus undamaged chromatin feature comparisons, significant differences were determined using two-sample Wilcoxon tests. The correlation between protein expression levels was analysed using Pearson *r* test. Overall survival was analysed by log-rank (Mantel–Cox) test. Data are presented as the means \pm s.d. All experiments were performed for at least three independent biological experiments unless indicated in the figure legends. Sample sizes were selected based on previous experience to ensure sufficient statistical power. For animal studies, power

analyses were performed using a web-based tool (www.biomath.info). In vivo experiments were not blinded during experimentation, although the labels were masked during data analysis.

Reporting summary

Further information on research design is available in the Nature Portfolio Reporting Summary linked to this article.

Data availability

Plasmids and primers used are listed in the Supplementary Information. CUT&Tag-seq and ATAC-seq data generated during this study are available at the Gene Expression Omnibus (GEO) under the accession number GSE288071. Mass spectrometry data are available via ProteomeXchange with the identifier PXD060714. Materials and reagents are available on request. Full immunoblots and gating of flow cytometry are provided as Supplementary Figs. 1 and 2. Source data are provided with this paper.

- Nabet, B. et al. The dTAG system for immediate and target-specific protein degradation. *Nat. Chem. Biol.* **14**, 431–441 (2018).
- Clouaire, T. et al. Comprehensive mapping of histone modifications at DNA double-strand breaks deciphers repair pathway chromatin signatures. *Mol. Cell* **72**, 250–262.e6 (2018).
- Smerdon, M. J. & Lieberman, M. W. Nucleosome rearrangement in human chromatin during UV-induced DNA-repair synthesis. *Proc. Natl Acad. Sci. USA* **75**, 4238–4241 (1978).
- Ortega, E. et al. Transcription factor dimerization activates the p300 acetyltransferase. *Nature* **562**, 538–544 (2018).
- Dombrowski, M., Engeholm, M., Dienemann, C., Dodonova, S. & Cramer, P. Histone H1 binding to nucleosome arrays depends on linker DNA length and trajectory. *Nat. Struct. Mol. Biol.* **29**, 493–501 (2022).

Acknowledgements This work was supported by grants from the National Natural Science Foundation of China (32090030 and 82430096), the National Key Research and Development Program of China (2023YFE0205200), the Shenzhen Municipal Commission of Science and Technology Innovation (JCYJ20220818100015032, JCYJ20220818100016034 and RCYX202170602040047), Shenzhen Medical Research Fund (B2302010) and the Shenzhen University 2035 Program for Excellent Research and Program for Youzuzhikeyan. We thank J. Luo, X. Xu, B. Liu, J. Yuan and M. Tan for their valuable suggestions; G. Legube for providing the AsiSI-ER-U2OS-AID cells; X. Xu for providing PARP1-KO, EJ5-U2OS and DR-U2OS cells; R. Greenberg for providing the U2OS-265 reporter cells; and J. Tamanini of ETediting, UK for English language editing before submission.

Author contributions Y.T., J.Z. and W.-G.Z. designed the experiments. Y.T., T.F., W.Z., M.L., W.T. and Y.Z. performed the molecular and biochemical experiments. Y.T., T.F. and Y.S. performed the mouse experiments. Y.T. and T.F. conducted the protein purification experiments. Y.T., T.F., J.Z., M.L. and F.C. performed the cellular irradiation experiments. Q.M. performed the sequencing analyses. M.T. and C.L. performed the sample analyses. S.T., Q.Z. and X.L. provided valuable suggestions for the design of experimental models. Y.T. and W.-G.Z. obtained the funding for this work. Y.T., T.F., J.Z. and W.-G.Z. wrote the manuscript.

Competing interests The authors declare no competing interests.

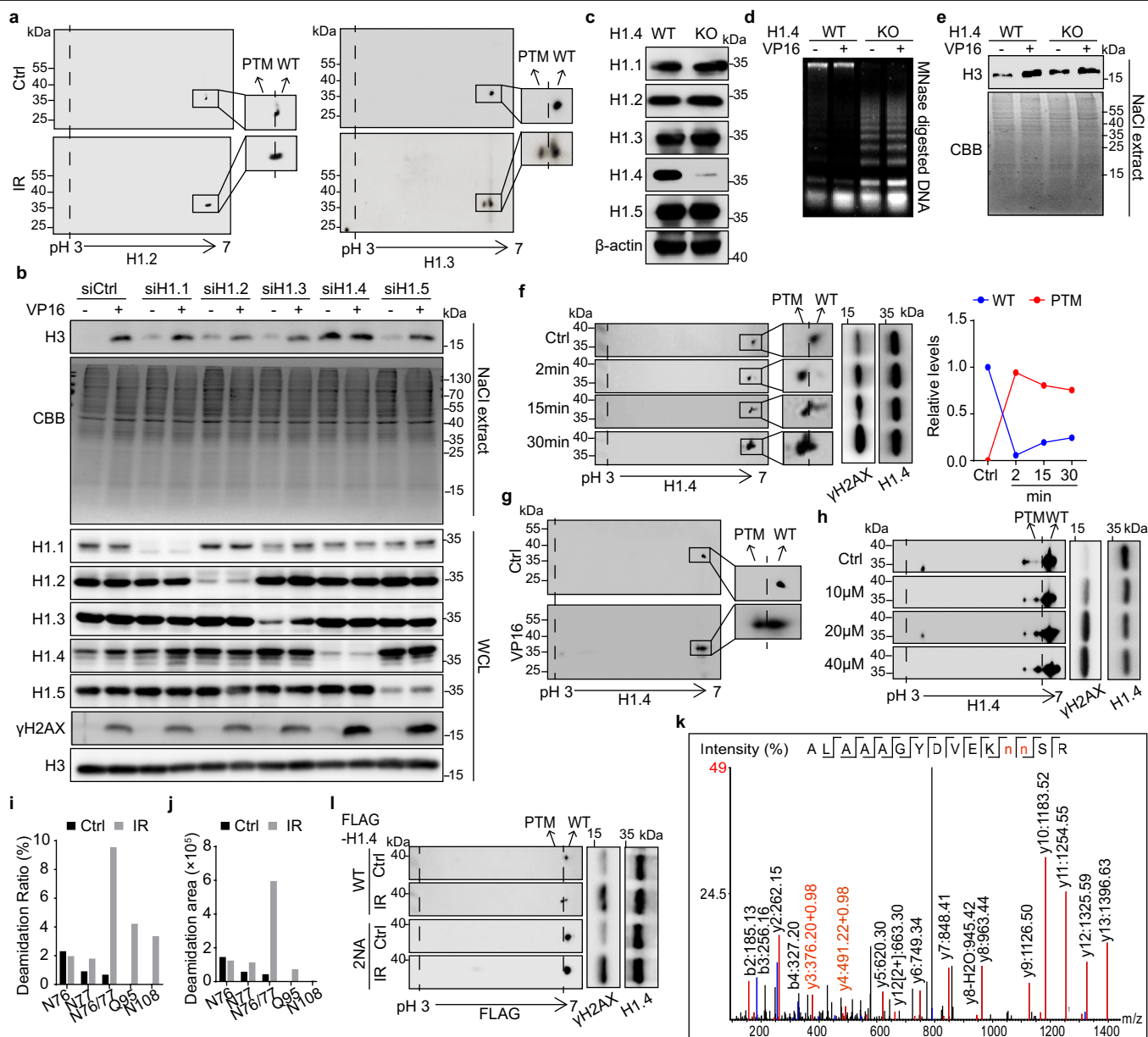
Additional information

Supplementary information The online version contains supplementary material available at <https://doi.org/10.1038/s41586-025-08835-0>.

Correspondence and requests for materials should be addressed to Wei-Guo Zhu.

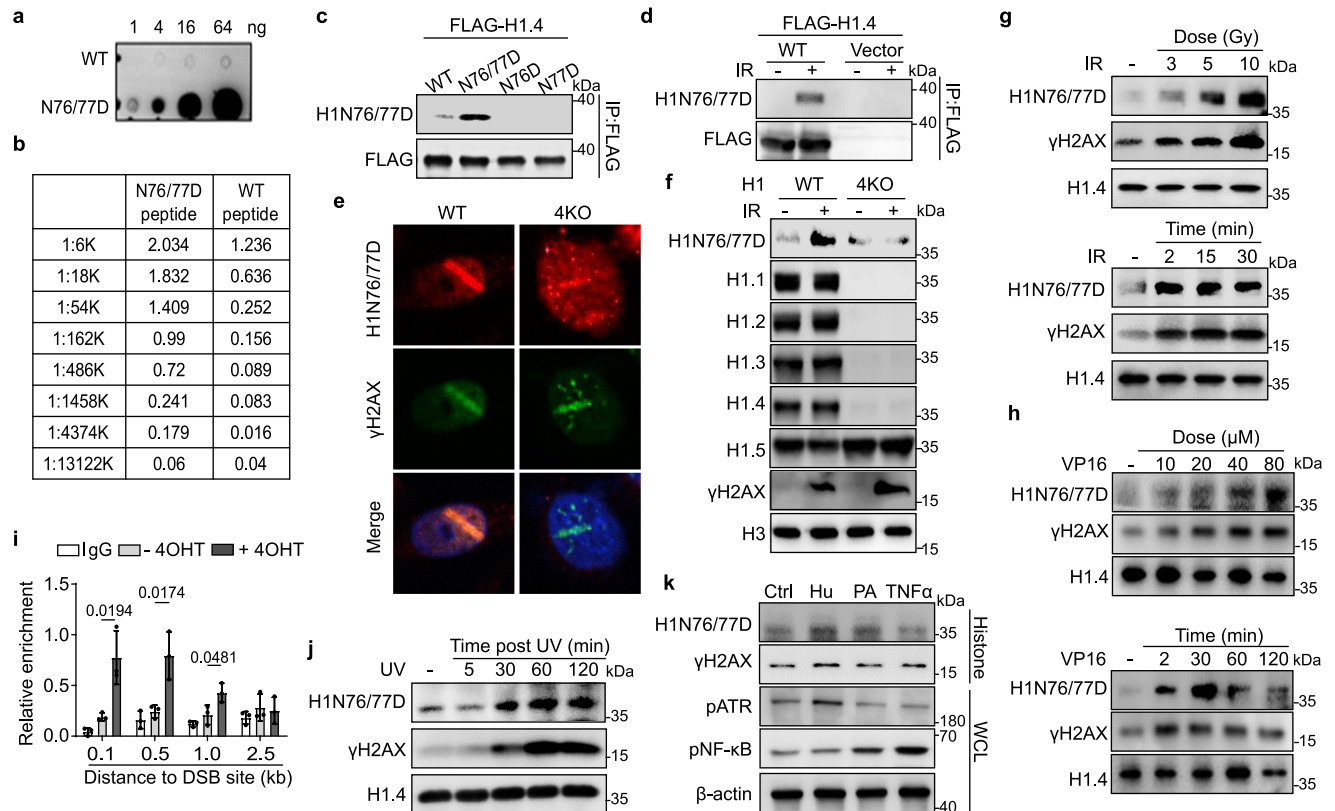
Peer review information Nature thanks Pinghui Feng, Guohong Li and the other, anonymous, reviewer(s) for their contribution to the peer review of this work. Peer reviewer reports are available.

Reprints and permissions information is available at <http://www.nature.com/reprints>.



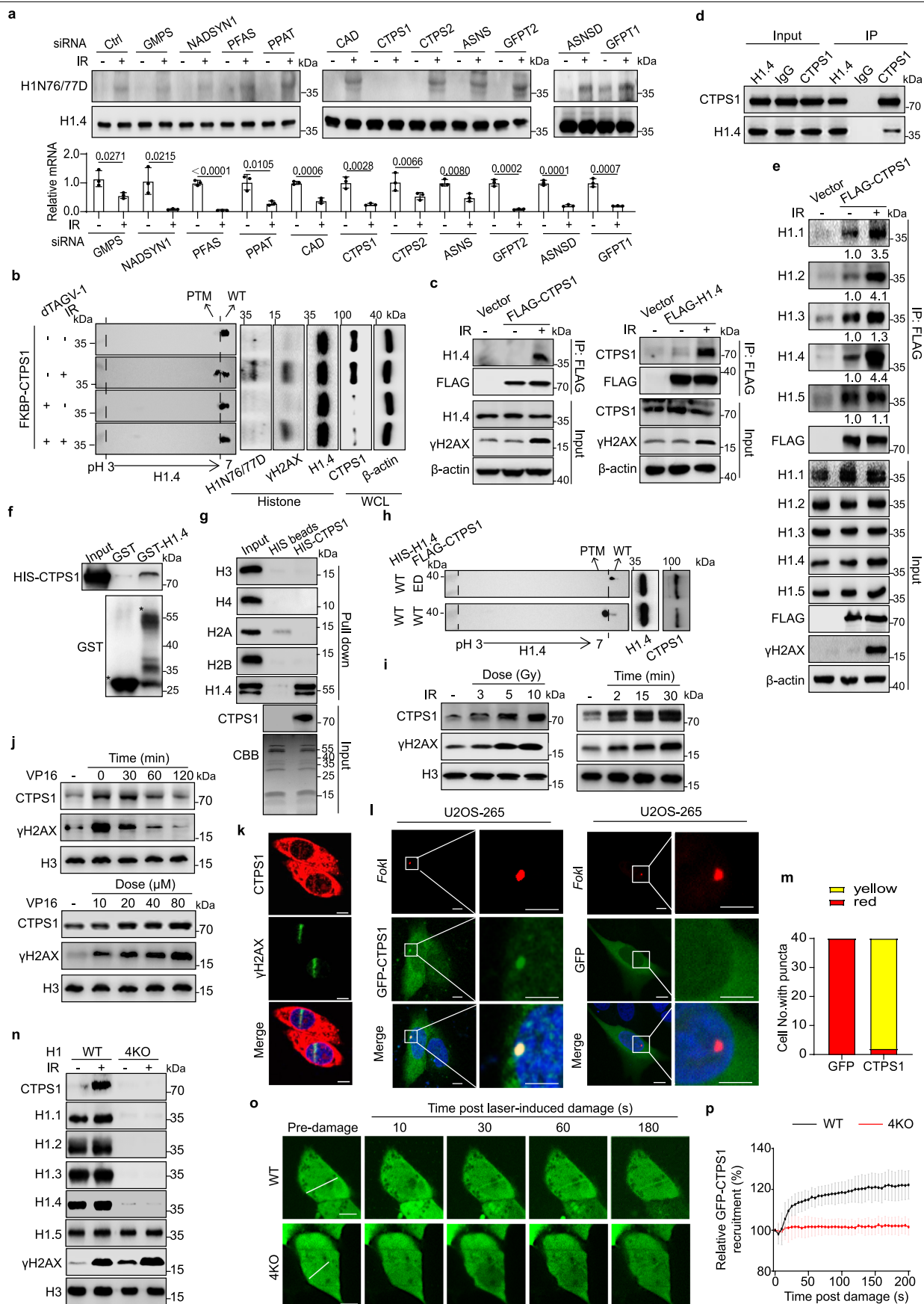
Extended Data Fig. 1 | DNA damage induces Deamidation of H1. **a**, HeLa cells were exposed to 10 Gy IR and released for 2 min. Histones were extracted for 2DGE. **b**, HeLa cells were transfected with the indicated siRNAs for 48 h and treated with or without VP16. Cell lysates were extracted using 1 M NaCl and analyzed by immunoblotting (top). WCLs were extracted and analyzed by immunoblotting (bottom). **c**, WCLs of WT or H1.4-KO HeLa cells were extracted and analyzed by immunoblotting. **d**, WT or H1.4-KO HeLa cells were treated with or without VP16. Chromatin fractions were extracted and analyzed by MNase sensitivity assay. **e**, WT or H1.4-KO HeLa cells were treated with or without VP16. Cell lysates were extracted using 1 M NaCl and analyzed by immunoblotting (top) and CBB (bottom). **f**, HeLa cells were exposed to 10 Gy IR and released for the indicated times. Histones were extracted for immunoblotting after 2DGE (left) or SDS-PAGE (middle). The relative quantification of H1.4 forms (WT and PTM) in the representative experiment is

shown (right). **g**, HeLa cells were exposed to 20 μM VP16 for 2 h. Histones were extracted for 2DGE. **h**, HeLa cells were exposed to the indicated doses of VP16 for 2 h. Histones were extracted for immunoblotting after 2DGE (left) or regular SDS-PAGE (right). **i, j**, HeLa cells were exposed to 10 Gy IR or not (Ctrl) and released for 2 min. Histones were extracted and deamidated peptides were identified by mass spectrometry (MS). Ratio (**i**) and relative quantification (**j**) of deamidated peptides are shown. **k**, The identification of N76 and N77 deamidated peptides by MS is shown. The product ions y3 (377.18) and y4 (492.20) indicated the deamidation of the asparagine at the 3rd and 4th position from the C terminus of the peptide. **l**, H1.4-KO HeLa cells transfected with the indicated FLAG-tagged plasmids (WT or 2NA) for 48 h were exposed to 10 Gy IR or not (Ctrl). Histones were extracted for immunoblotting after 2DGE (left) or regular SDS-PAGE (right). Three independent experiments were performed in (**a-j**).



Extended Data Fig. 2 | Deamidation of H1N76/77 is increased after DNA damage. **a**, Dot blot analysis of the indicated amounts of peptides using a purified H1N76/77D antibody diluted 1:1,000. The sensitivity of the purified anti-H1N76/77D antibody was <1 ng. Dot blot using indicated peptides showing that anti-H1N76/77D only recognized 2ND peptides, not WT peptides. **b**, ELISA confirmation that the specificity of the purified anti-H1N76/77D antibody against the immunogens was 27-fold higher than of unmodified (WT) peptide. **c**, WCLs of H1.4-KO HeLa cells with stable expression of WT or mutant FLAG-H1.4 were extracted, immunoprecipitated using anti-FLAG, and analyzed by immunoblotting. The H1N76/77D antibody specifically recognized double-deamidated H1 and did not interact with single-deamidated H1.4. **d**, H1.4-KO HeLa cells with stable expression of H1.4-WT or vector control were treated with 10 Gy IR. WCLs were extracted, immunoprecipitated using anti-FLAG, and analyzed by immunoblotting. The H1N76/77D antibody specifically recognized double-deamidated H1 and did not interact with FLAG-Vector immunoprecipitants. **e**, WT or quadruple H1 variant-knockout (H1.1-H1.4 KO; 4KO) HeLa cells were micro-irradiated and analyzed by immunofluorescence at

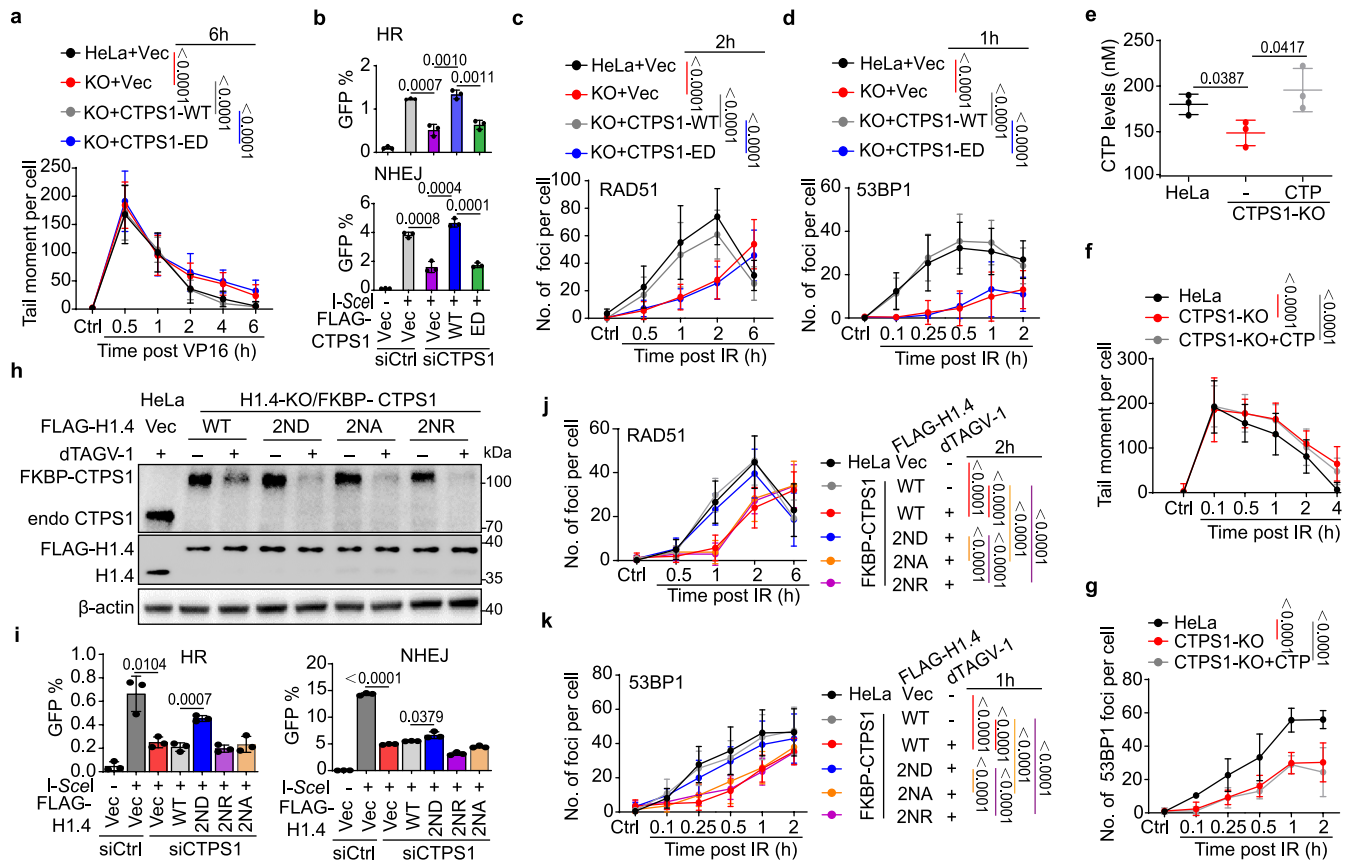
5 min post-irradiation. Scale bars, 5 μ m. **f**, WT or 4KO HeLa cells were exposed to 10 Gy IR and released for 5 min. Histones were extracted for immunoblotting. **g**, HeLa cells were exposed to the indicated doses of IR and released for 2 min (top), or exposed to 10 Gy IR and released for the indicated times (bottom). Histones were extracted for immunoblotting. **h**, HeLa cells were exposed to the indicated doses of VP16 for 2 h (top) or exposed to 20 μ M VP16 for 2 h and released for indicated times (bottom). Histones were extracted for immunoblotting. **i**, U2OS-AsiSi-ER-AID cells were treated with or without 4OHT (500 nM) for 4 h and subjected to chromatin immunoprecipitation (ChIP) with anti-IgG or anti-H1N76/77D followed by real-time PCR analysis. **j**, HeLa cells were exposed to ultraviolet radiation C (UVC, 20 J/cm²), then released for the indicated times. Histones were extracted for immunoblotting. **k**, HeLa cells were exposed to 8 mM hydroxyurea (Hu) for 3 h, 0.2 mM palmitic acid (PA) for 24 h, or 0.1 μ g/mL TNF- α for 5 h. Histones and WCLs were extracted for immunoblotting. Data represent the means \pm s.d. $n = 3$ samples (**i**) from three independent experiments. P values were calculated using Student unpaired two-tailed t-tests (**i**). Three independent experiments were performed (**a-k**).



Extended Data Fig. 3 | See next page for caption.

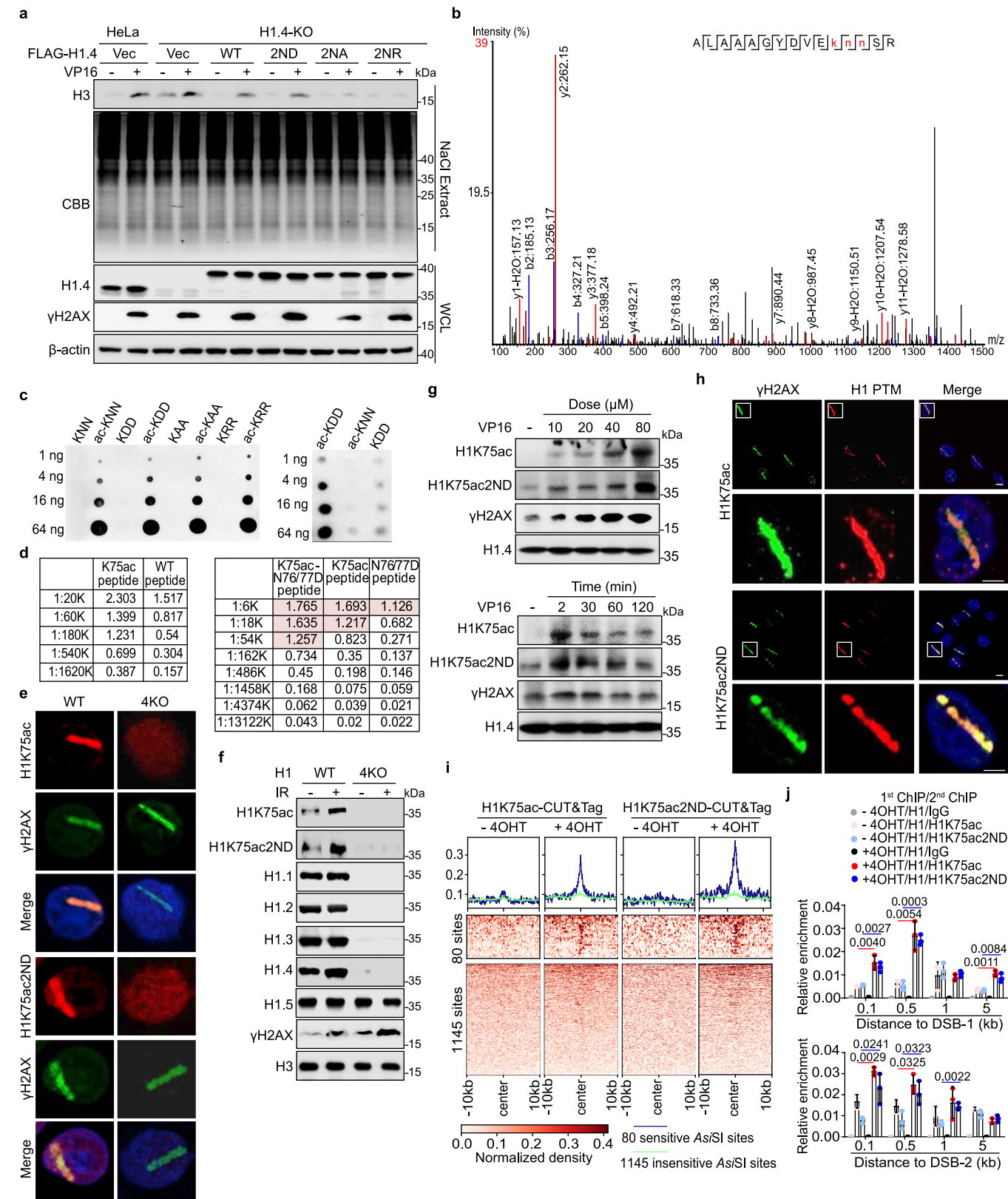
Extended Data Fig. 3 | CTPS1 deamidates H1 N76/77 in response to DNA damage. **a**, HeLa cells were transfected with control siRNA (siCtrl) or siRNA targeting individual GATs for 48 h and then exposed or not to 10 Gy IR. Histones were extracted for immunoblotting (top). RNA from cells without IR was extracted for real-time PCR to validate the knockdown efficiency (bottom). **b**, HeLa cells expressing FKBP-CTPS1 were treated with dTAGV-1 (1 mM) for 3 h and then exposed to 10 Gy IR. WCLs or histones were extracted for immunoblotting after 2DGE (left) or regular SDS-PAGE (right). **c,d**, HeLa cells were transfected with FLAG-CTPS1 (**c** left) or FLAG-H1.4 (**c** right) with or without 10 Gy IR (**c**) or all exposed to 10 Gy IR (**d**). WCLs were immunoprecipitated using anti-FLAG (**c**) or anti-IgG, anti-H1.4, or anti-CTPS1 (**d**) and analyzed by immunoblotting. **e**, HeLa cells were transfected with FLAG-CTPS1 for 48 h and exposed or not to 10 Gy IR. WCLs were extracted, immunoprecipitated with anti-FLAG, and analyzed by immunoblotting. The relative quantifications of the binding intensities are indicated below each band. **f**, GST or GST-H1.4 recombinant proteins were incubated with HIS-CTPS1 for GST pull-down assays; * indicates specific protein bands. **g**, Histone octamer and GST-H1.4 recombinant proteins were mixed and incubated with HIS-CTPS1 for pull-down assay using HIS beads (top). CBB staining shows the input (bottom). **h**, HIS-H1.4-WT purified from *E. coli* was incubated with or without FLAG-CTPS1-WT or FLAG-CTPS1-ED purified from HEK293T cells. Immunoblots of in vitro deamidation reactions analyzed after 2DGE (left) and regular SDS-PAGE (right)

are shown. **i**, HeLa cells were exposed to the indicated doses of IR and released for 2 min (left), or exposed to 10 Gy IR and released for indicated times (right). Chromatin was extracted for immunoblotting. **j**, HeLa cells were exposed to 20 μ M VP16 for 2 h and released for the indicated times (top) or to the indicated doses of VP16 for 2 h (bottom). Chromatin was extracted for immunoblotting. **k**, HeLa cells were micro-irradiated, fixed at 5 min post-irradiation, and analyzed by immunofluorescence using anti-CTPS1 (red) and anti- γ H2AX (green). **l,m**, U2OS-265 reporter cells were transfected with GFP-CTPS1 plasmid (left) or GFP vector (right) for 48 h and treated with 4OHT (500 nM) and shield I (30 ng/mL) for 6 h. Co-localization of *FokI*-mCherry (red) and GFP-CTPS1 (green) was analyzed by immunofluorescence (**l**). Quantifications of 40 cells from three independent experiments are shown (**m**). **n**, WT or 4KO HeLa cells were exposed to 10 Gy IR and released for 5 min. Chromatin fractions were extracted for immunoblotting. **o,p**, WT or 4KO HeLa cells were transfected with GFP-CTPS1 for 48 h, then micro-irradiated. Images were captured every 10 s for 5 min. Representative images (**o**) and quantification of 30 cells from three independent experiments (**p**) are shown. Data represent the means \pm s.d. (**a**, **p**) and values (**m**). $n = 3$ samples (**a**), $n = 40$ cells (**m**) or $n = 30$ cells (**p**) from three independent experiments. P values were calculated using Student unpaired two-tailed t-tests (**a**). Scale bars, 5 μ m (**k**, **l**, **o**). Three independent experiments were performed in (**a**-**k**, **m**, **n**).



Extended Data Fig. 4 | CTPS1 deamidated-H1N76/77 is required for DNA damage repair. **a**, WT or CTPS1-KO HeLa cell lines stably expressing WT or mutant CTPS1 were exposed to VP16 and analyzed by comet assay at the indicated times post-treatment. Statistical analyses of the tail moment at 6 h post treatment are shown. **b**, pDR-GFP (top) or pEJ5-GFP (bottom) U2OS cells were transfected with the indicated siRNAs and then plasmids, and then infected with a retrovirus expressing I-SceI, before flow cytometric analysis of GFP expression. **c,d**, WT or CTPS1-KO HeLa cell lines stably expressing WT or mutant CTPS1 were exposed to 10 Gy IR and analyzed by immunofluorescence at the indicated times post-treatment. Statistical analyses of RAD51 (**c**) and 53BP1 (**d**) foci numbers at indicated time points post-IR are shown. **e**, WT or CTPS1-KO HeLa cell lines were treated with or without 200 μ M CTP for 2 h. Cells were collected and analyzed by mass spectrometry to determine CTP levels. **f,g**, WT or CTPS1-KO HeLa cell lines were treated with or without 200 μ M CTP for 2 h and exposed to 10 Gy IR and analyzed by comet assays (**f**) or

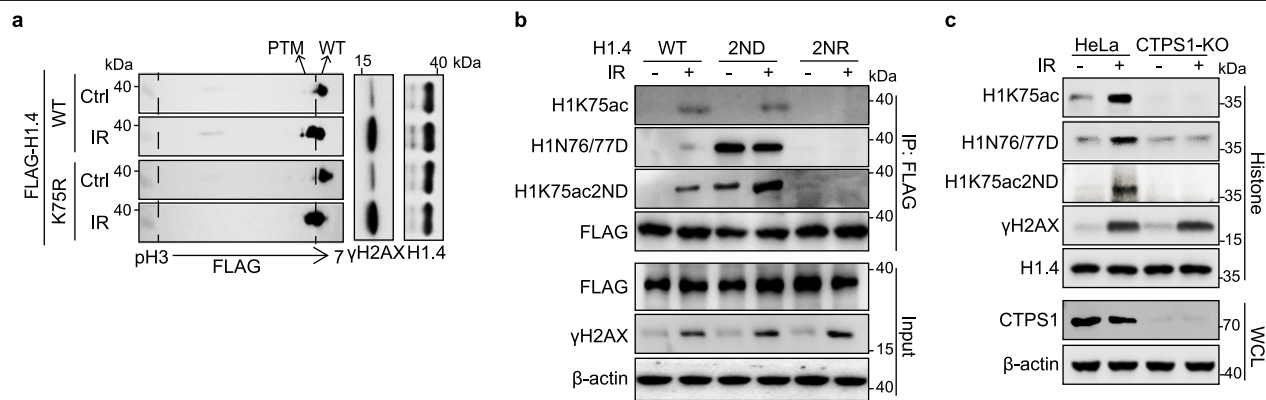
immunofluorescence to detect 53BP1 foci (**g**) post-IR. Statistical analyses of the tail moment at 4 h (**f**) or foci numbers at the 1 h (**g**) post-IR are shown. **h**, H1.4-KO HeLa cells stably expressing WT or mutant FLAG-H1.4 were modified to express FKBP-CTPS1, and treated with dTAGV-1 for 3 h. WCLs were extracted and analyzed by immunoblotting. **i**, pDR-GFP (left) or pEJ5-GFP (right) U2OS cells were transfected with the indicated siRNAs, then with plasmids, and flow cytometric analysis of GFP expression was performed. **j,k**, H1.4-KO HeLa cells stably expressing WT or mutant FLAG-H1.4 were modified to express FKBP-CTPS1, treated with dTAGV-1 for 3 h, and exposed to 10 Gy IR. Cells were fixed and analyzed by immunofluorescence at the indicated times post-treatment. Statistical analyses of RAD51 (**j**) and 53BP1 (**k**) foci numbers at 2 h or 1 h post-treatment are shown. Data represent the means \pm s.d. (**a-g, i-k**). $n = 3$ samples (**b, e, i**) or $n = 50$ cells (**a, c, d, f, g, j, k**) each group from three independent experiments. P values were calculated using Student unpaired two-tailed t-tests (**a-g, i-k**). Three independent experiments were performed (**a-g**).



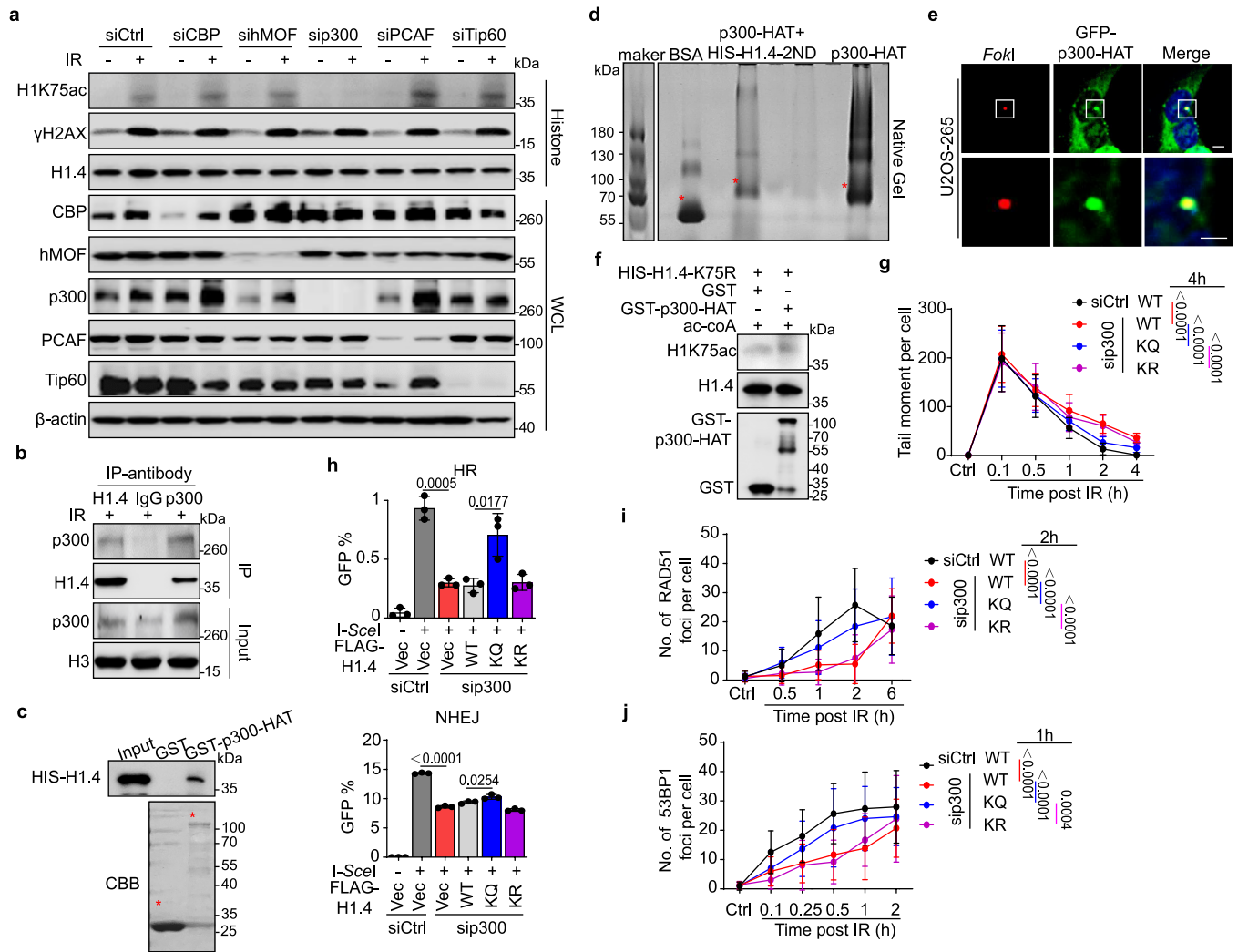
Extended Data Fig. 5 | See next page for caption.

Extended Data Fig. 5 | DNA damage induces H1K75 acetylation. **a**, WT or H1.4-KO HeLa cells with stable expression of FLAG-tagged WT or mutant H1.4 were treated with or without VP16. Cell lysates were extracted using 1 M NaCl and analyzed by immunoblotting (top) and CBB (middle). WCLs were analyzed by immunoblotting (bottom). **b**, HeLa cells were exposed to 10 Gy IR, released for 2 min, and histones were extracted. K75 acetylated and N76/N77 deamidated peptides were simultaneously identified by MS. **c**, Dot blot analysis of the indicated amounts of peptides using purified anti-H1K75ac (left) or anti-H1K75ac2ND (right) antibody diluted 1:1,000. The sensitivities of the purified antibodies were <1 ng. **d**, ELISA confirmation that the specificity of the purified H1K75ac (left) and H1K75ac2ND (right) antibodies against the immunogens was >4-fold higher than that of unmodified peptides. **e**, WT or 4KO HeLa cells were micro-irradiated and analyzed by immunofluorescence at 5 min post-irradiation.

f, WT or 4KO HeLa cells were exposed or not to 10 Gy IR and released for 5 min. Histones were extracted for immunoblotting. **g**, HeLa cells were exposed to the indicated doses of VP16 for 2 h (top) or to 20 μ M VP16 for 2 h and released for the indicated times (bottom). Histones were extracted for immunoblotting. **h**, HeLa cells were analyzed for γ H2AX (green) and H1 PTM (red) by immunofluorescence at 5 min post-micro-irradiation. **i**, U2OS-AsiSI-ER-AID cells were treated with or without 4OHT and subjected to CUT&Tag-seq with anti-H1K75ac or anti-H1K75ac2ND. **j**, U2OS-AsiSI-ER-AID cells were treated with or without 4OHT and subjected to ChIP-re-ChIP with indicated antibodies. Data represent the means \pm s.d. (**j**). $n = 3$ samples from three independent experiments (**j**). P values were calculated using Student unpaired two-tailed t-tests (**j**). Three independent experiments were performed in (**a**, **c-j**). Scale bars, 5 μ m (**e**, **h**).



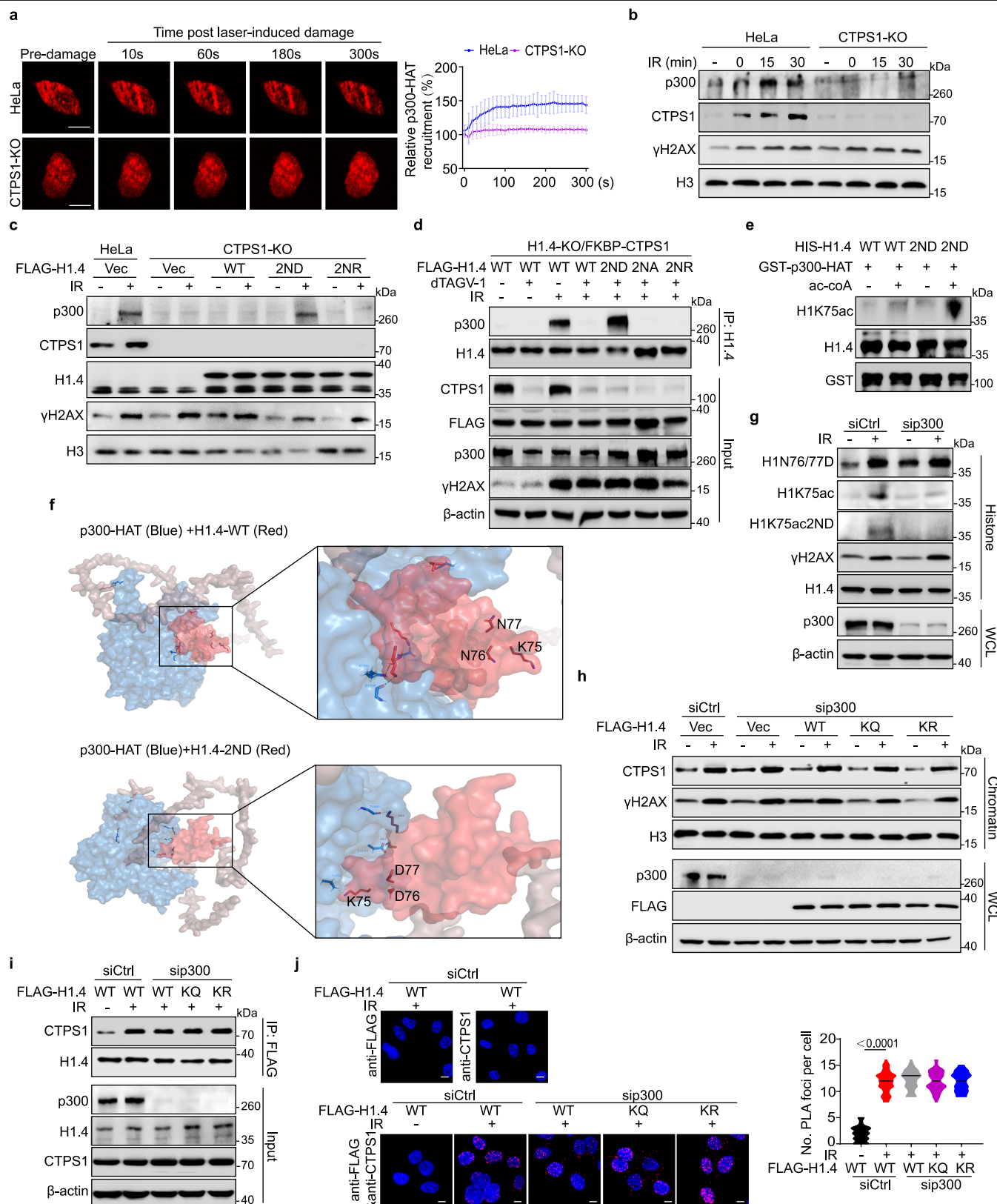
Extended Data Fig. 6 | H1K75 acetylation does not influence H1N76/77 deamidation. a, H1.4-KO HeLa cells transfected with the indicated plasmids for 48 h and then exposed to 10 Gy IR. Histones were extracted for immunoblotting after 2DGE (left) or regular SDS-PAGE (right). **b**, H1.4-KO HeLa cells were transfected with H1.4-WT, -2ND, or -2NR plasmids for 48 h and exposed to 10 Gy IR. WCLs were extracted, immunoprecipitated using anti-FLAG, and analyzed by immunoblotting. **c**, WT or CTPS1-KO HeLa cells were exposed to 10 Gy IR. Histones or WCLs were extracted and analyzed by immunoblotting. Three independent experiments were performed in (a-c).



Extended Data Fig. 7 | p300 acetylates H1K75 in response to DNA damage.

a, HeLa cells were transfected with the indicated siRNAs for 48 h, and exposed or not to 10 Gy IR. Histones and WCLs were extracted and analyzed by immunoblotting. **b**, HeLa cells were exposed to 10 Gy IR. WCLs were extracted; immunoprecipitated using anti-IgG, anti-H1.4, or anti-p300; and analyzed by immunoblotting. **c**, Recombinant GST or GST-p300-HAT proteins were incubated with HIS-H1.4 for GST pull-down assays; *indicates specific protein bands identified by CBB staining. **d**, p300-HAT protein was incubated with or without HIS-H1.4-2ND for 1 h and subjected to native PAGE. Bovine serum albumin (BSA) was loaded as a molecular weight reference. **e**, U2OS-265 reporter cells were transfected with GFP-p300-HAT plasmid for 48 h, and treated with 4OHT (500 nM) and shield I (30 ng/ml) for 6 h. The co-localization of FokI-mCherry (red) and GFP-p300-HAT (green) was analyzed by immunofluorescence. Scale bars, 5 μm. **f**, GST or GST-p300-HAT was subjected to in vitro acetylation

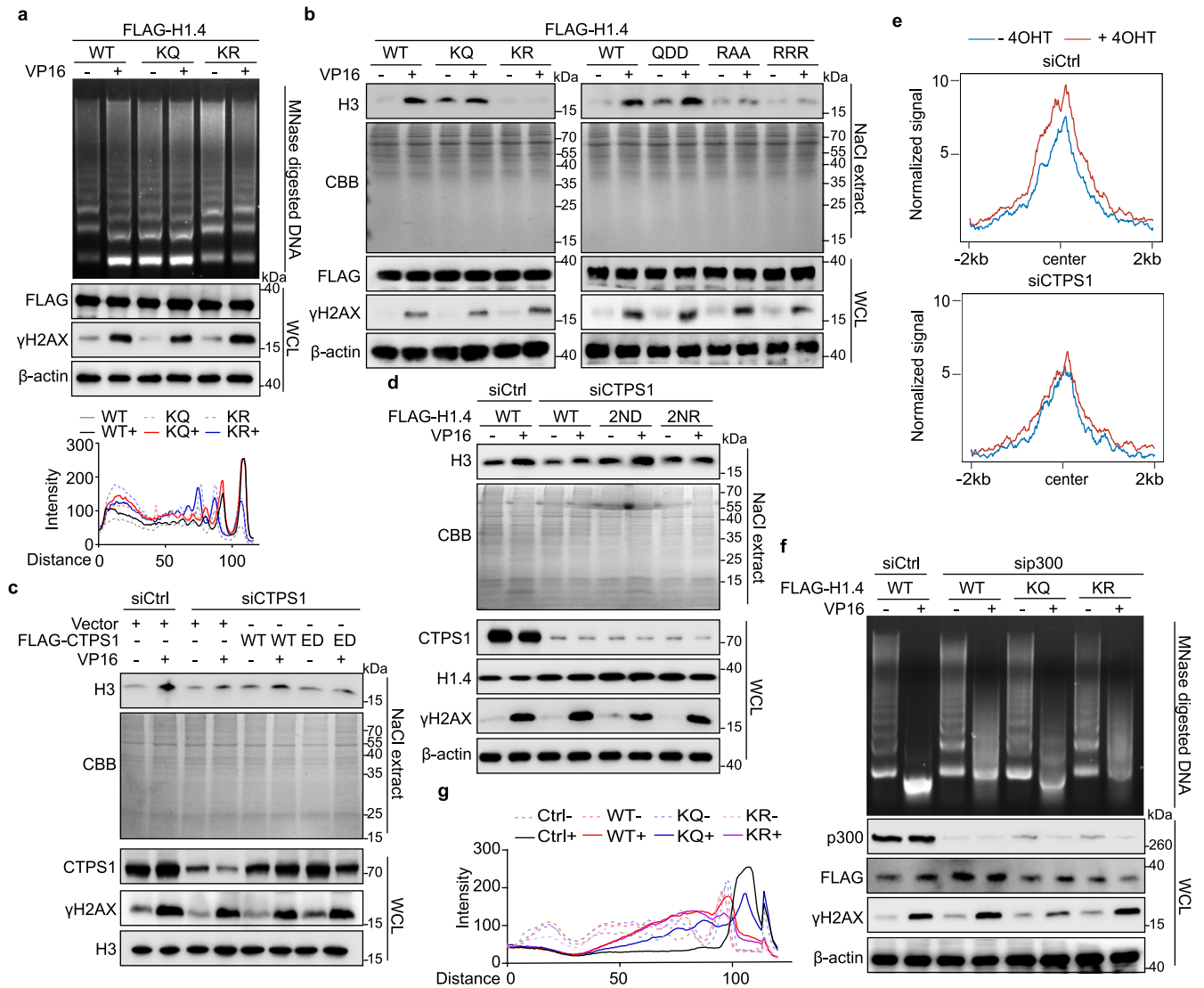
assay using HIS-H1.4-K75R protein purified from *E. coli* as substrate. **g**, H1.4-KO HeLa cells stably expressing WT or mutant H1.4 were transfected with the indicated siRNAs, exposed to 10 Gy IR, and analyzed by comet assay at the indicated times post-IR. **h**, pDR-GFP (top) or pEJ5-GFP (bottom) U2OS cells were transfected with the indicated siRNAs, followed by plasmids, and flow cytometric analysis of GFP expression was performed. **i, j**, H1.4-KO HeLa cells stably expressing WT or mutant H1.4 were transfected with the indicated siRNAs, exposed to 10 Gy IR, and analyzed by immunofluorescence at the indicated times post-IR. Quantifications of RAD51 (**i**) and 53BP1 (**j**) foci numbers per cell from 50 cells are shown. Data represent the means ± s.d. (**g-j**). $n = 3$ samples (**h**) and $n = 50$ cells (**g, i, j**) in each group from three independent experiments (**g-j**). P values were calculated using Student unpaired two-tailed t-tests (**g-j**). Three independent experiments were performed in (**a-j**).



Extended Data Fig. 8 | See next page for caption.

Extended Data Fig. 8 | H1N76/77 deamidation promotes p300 binding to chromatin and H1K75 acetylation. **a**, WT or CTPSI-KO HeLa cells were transfected with an mCherry-p300-HAT plasmid and exposed to laser micro-irradiation. Images were captured every 10 sec for 5 min (left), and the irradiated path signal intensity in cells was calculated (right). **b**, WT or CTPSI-KO HeLa cells were exposed to 10 Gy IR and released for the indicated times. Chromatin was extracted and analyzed by immunoblotting. **c**, WT or CTPSI-KO HeLa cells were transfected with the indicated plasmids and exposed or not to 10 Gy IR. Chromatin was extracted and analyzed by immunoblotting. **d**, H1.4-KO HeLa cells stably expressing WT or mutant FLAG-H1.4 were modified to express FKBP-CTPSI, treated with dTAGV-1 for 3 h, and exposed to 10 Gy IR. WCLs were extracted, immunoprecipitated using anti-H1.4, and analyzed by immunoblotting. **e**, Recombinant GST-p300-HAT protein was subjected to in vitro acetylation assay using HIS-H1.4-WT or HIS-H1.4-2ND proteins purified from *E. coli* as substrates. **f**, Molecular-docking-predicted 3D structural image of interaction between p300 and H1.4 by GRAMM (gramm.compbio.ku.edu) in H1.4-WT (top) and H1.4-2ND (bottom) contexts. Locations of the main

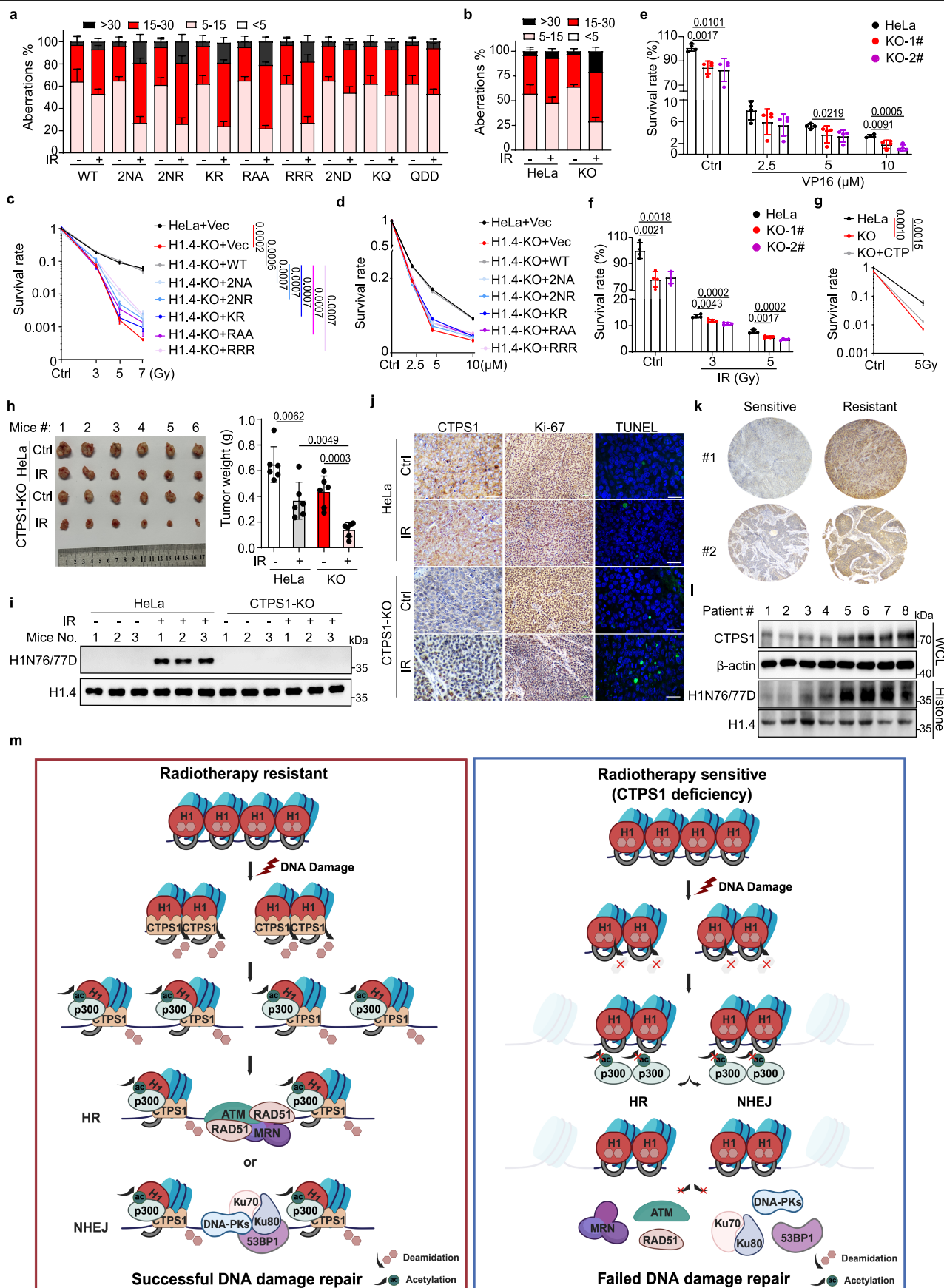
interacting amino acids are shown, and residues 75, 76, and 77 are marked. Blue, p300-HAT domain; red, H1.4 globular domain; light red, H1.4 C and N terminals. **g**, HeLa cells were transfected with indicated siRNAs for 48 h and exposed to 10 Gy IR. Extracted histones or WCLs were analyzed by immunoblotting. **h**, H1.4-KO HeLa cells were transfected with the indicated siRNAs and then plasmids for 48 h, and exposed to 10 Gy IR. Chromatin and WCLs were extracted and analyzed by immunoblotting. **i**, H1.4-KO HeLa cells were transfected with siRNA and the indicated plasmids for 48 h and exposed to 10 Gy IR. WCLs were extracted, immunoprecipitated using anti-FLAG, and analyzed by immunoblotting. **j**, H1.4-KO HeLa cells were transfected with the indicated siRNA and plasmids for 48 h, and exposed to 10 Gy IR. PLAs were performed using anti-FLAG or/and anti-CTPSI. Representative images (left) and quantification of 50 cells each group (right) are shown. Data represent the means \pm s.d. (**a,j**). $n = 8$ (**a**) or $n = 50$ (**j**) cells in each group from three independent experiments. P values were calculated using Student unpaired two-tailed t-tests (**j**). Three independent experiments were performed in (**a-e, g-i**). Scale bars, 5 μ m (**a,j**).



Extended Data Fig. 9 | Sequential H1N76/77 deamidation and H1K75 acetylation promotes chromatin relaxation and maintains genome stability.

a, H1.4-KO HeLa cells were transfected with the indicated plasmids for 48 h and treated with or without VP16. Chromatin fractions were extracted and analyzed by MNase sensitivity assay (top). WCLs were extracted and analyzed by immunoblotting (middle). The intensity of each lane was quantified (bottom). **b**, H1.4-KO HeLa cells stably expressing FLAG-tagged WT or mutant H1.4 were treated with or without VP16. Cell lysates were extracted using 1 M NaCl and analyzed by immunoblotting (top) and CBB (middle). WCLs were extracted and analyzed by immunoblotting (bottom). **c**, HeLa cells were transfected with the indicated siRNAs and plasmids for 48 h and treated or not with VP16. Cell lysates were extracted using the indicated dose of NaCl buffer and analyzed by immunoblotting (top) and CBB (middle). WCLs were extracted and analyzed by

immunoblotting (bottom). **d**, H1.4-KO HeLa cells were transfected with the indicated siRNAs and plasmids for 48 h and treated with or without VP16. Cell lysates were extracted using 1 M NaCl and analyzed by immunoblotting (top) and CBB (middle). WCLs were extracted and analyzed by immunoblotting (bottom). **e**, U2OS-AsiSI-ER-AID cells were transfected with the indicated siRNAs for 48 h and then treated with or without 4OHT. Cells were collected and subjected to ATAC-seq, and 80 sensitive DSB sites were plotted. **f, g**, H1.4-KO HeLa cells were transfected with siRNA control (siCtrl) or sip300, then plasmids for 48 h, and treated with or without VP16. Chromatin fractions were extracted and analyzed by MNase sensitivity assay (**f** top). WCLs were extracted and analyzed by immunoblotting (**f** bottom). The intensity of each lane was quantified (**g**). Three independent experiments were performed in (**a-f**).



Extended Data Fig. 10 | See next page for caption.

Article

Extended Data Fig. 10 | CTPS1 is a potential therapeutic target for cancer.

a, H1.4-KO HeLa cells with stable expression of H1.4 WT or mutants were exposed or not to 3 Gy IR and subjected to metaphase assay. Chromosomes were counterstained with Giemsa and the aberrations were quantified. **b**, WT or CTPS1-KO HeLa cells were exposed or not to IR and subjected to metaphase assay. Chromosomes were counterstained with Giemsa and the aberrations were quantified. **c,d**, WT or H1.4-KO HeLa cell lines stably expressing WT or mutant H1.4 were subjected to colony formation assay after IR (**c**) or VP16 (**d**) exposure. Statistical analyses of survival rates at the last dose are shown. **e,f**, WT or two CTPS1-KO HeLa cell lines were subjected to colony formation assay after VP16 (**e**) or IR (**f**) exposure and the survival rate was quantified. **g**, WT or CTPS1-KO HeLa cell lines were treated with or without 200 μ M CTP for 2 h and exposed to IR. Cells were sub-seeded for colony formation assay and the survival rate was quantified. **h-j**, WT or CTPS1-KO HeLa cells were injected into nude mice, followed by treatment with or without IR (n = 6 per group). Tumor images (**h** left) and tumor weights (**h** right) of xenografts are shown. Immunoblots of extracted histones (**i**), and representative immunohistochemistry and

TUNEL staining images of xenografts (**j**) are shown. Scale bars, 50 μ m.

k, Representative immunohistochemistry images of CTPS1 expression in cervical cancer tissues isolated from patients before exposure to radiotherapy. Sensitive, patients who were survived after 5 years post radiotherapy; Resistant, patients who were dead within 5 years post radiotherapy. **l**, Representative western blot images of CTPS1 and H1N76/77D expression in 8 cervical cancer tissues isolated from patients after exposure to radiotherapy. **m**, Model of H1N76/77D-mediated regulation of chromatin structure in the context of DNA damage. Deamidation of H1N76/77 catalyzed by CTPS1 is prerequisite for a sequential binding of histone acetyltransferase p300 to the reaction site of H1K75. This specific H1K75 acetylation is well associated with an opening structure of damaged chromatin and is therefore beneficial for DNA damage repair factors loading onto the DNA damage sites. The working model was created using BioRender (<https://biorender.com>). Data represent the means \pm s.d. (**a-c**, **e-h**) or means (**d**). n = 5 fields (**a,b**), n = 3 samples (**c,g**), n = 2 (**d**) samples, or n = 4 samples (**e,f**) from three independent experiments. P values were calculated using Student unpaired two-tailed t-tests (**c-h**). Scale bars, 50 μ m (**j**).

Reporting Summary

Nature Portfolio wishes to improve the reproducibility of the work that we publish. This form provides structure for consistency and transparency in reporting. For further information on Nature Portfolio policies, see our [Editorial Policies](#) and the [Editorial Policy Checklist](#).

Statistics

For all statistical analyses, confirm that the following items are present in the figure legend, table legend, main text, or Methods section.

n/a	Confirmed
<input type="checkbox"/>	<input checked="" type="checkbox"/> The exact sample size (<i>n</i>) for each experimental group/condition, given as a discrete number and unit of measurement
<input type="checkbox"/>	<input checked="" type="checkbox"/> A statement on whether measurements were taken from distinct samples or whether the same sample was measured repeatedly
<input type="checkbox"/>	<input checked="" type="checkbox"/> The statistical test(s) used AND whether they are one- or two-sided <i>Only common tests should be described solely by name; describe more complex techniques in the Methods section.</i>
<input type="checkbox"/>	<input checked="" type="checkbox"/> A description of all covariates tested
<input type="checkbox"/>	<input checked="" type="checkbox"/> A description of any assumptions or corrections, such as tests of normality and adjustment for multiple comparisons
<input type="checkbox"/>	<input checked="" type="checkbox"/> A full description of the statistical parameters including central tendency (e.g. means) or other basic estimates (e.g. regression coefficient) AND variation (e.g. standard deviation) or associated estimates of uncertainty (e.g. confidence intervals)
<input type="checkbox"/>	<input checked="" type="checkbox"/> For null hypothesis testing, the test statistic (e.g. <i>F</i> , <i>t</i> , <i>r</i>) with confidence intervals, effect sizes, degrees of freedom and <i>P</i> value noted <i>Give P values as exact values whenever suitable.</i>
<input checked="" type="checkbox"/>	<input type="checkbox"/> For Bayesian analysis, information on the choice of priors and Markov chain Monte Carlo settings
<input checked="" type="checkbox"/>	<input type="checkbox"/> For hierarchical and complex designs, identification of the appropriate level for tests and full reporting of outcomes
<input type="checkbox"/>	<input checked="" type="checkbox"/> Estimates of effect sizes (e.g. Cohen's <i>d</i> , Pearson's <i>r</i>), indicating how they were calculated

Our web collection on [statistics for biologists](#) contains articles on many of the points above.

Software and code

Policy information about [availability of computer code](#)

Data collection	<p>All softwares are commercially or freely available.</p> <ol style="list-style-type: none">1.Western Blot's proteins were visualized with a Tanon 5200SF Imaging System.2.The MS/MS raw data were processed for protein identification and PTM analysis using PEAKS Studio 8.5.3.Comet assay' images were captured using an Olympus BX51 fluorescent microscope.4.Immunofluorescent images were captured under a Nikon confocal microscope.5.For the laser assay, cells were locally irradiated with a 365-nm pulsed nitrogen UV laser (16 Hz pulse, 41% laser output) generated from a MicroPoint system (Andor).6.ChIP qPCR and ChIP-re-ChIP were performed using a qTOWER3G Touch Real-Time PCR Detection System.7.For chromosome aberration assay, the images were obtained using a DragonFly confocal imaging system.8.For molecular docking, histone H1.4 or H1.4-2ND were predicted by AlphaFold2. GRAMM and PyMol were used for virtual verification.9.Flow cytometry data was collected using FlowJo CE and analyzed using FlowJo™ v7.6.5 software.10.For CUT&Tag-seq analysis, raw sequencing data was aligned to the GRhg38 (hg38) genome build using Bowtie2 (v2.3.4.1).11. All libraries were sequenced by illumina NovoSeq 6000. <p>The software used for data collection was described in "Method". No special code were used.</p>
Data analysis	<p>All softwares are commercially or freely available.</p> <ol style="list-style-type: none">1.Comet tail moments were measured using the OpenComet plugin in ImageJ.2.For Microscale thermophoresis, curve fitting was performed by using MO. Affinity Analysis.3.Image J was used to analyze Immunfluorescence images.4.For laser assay, the intensity of the irradiation path signal was calculated using ImageJ.5.PLA foci were automatically quantified using ImageJ software.

6. For MNase, the intensity of each lane was analyzed using ImageJ.
7. Statistical Analysis was done in PRISM 9.
8. Figures were compiled using Adobe Illustrator.

For manuscripts utilizing custom algorithms or software that are central to the research but not yet described in published literature, software must be made available to editors and reviewers. We strongly encourage code deposition in a community repository (e.g. GitHub). See the Nature Portfolio [guidelines for submitting code & software](#) for further information.

Data

Policy information about [availability of data](#)

All manuscripts must include a [data availability statement](#). This statement should provide the following information, where applicable:

- Accession codes, unique identifiers, or web links for publicly available datasets
- A description of any restrictions on data availability
- For clinical datasets or third party data, please ensure that the statement adheres to our [policy](#)

Plasmids and primers used are listed in the Supplementary Information. CUT&Tag-seq and ATAC-seq data generated during this study are available at the Gene Expression Omnibus under accession number GSE288071. Source data are provided with this paper.

Research involving human participants, their data, or biological material

Policy information about studies with [human participants or human data](#). See also policy information about [sex, gender \(identity/presentation\)](#), [and sexual orientation](#) and [race, ethnicity and racism](#).

Reporting on sex and gender	Sex and gender were not considered in this study and this information was not collected as part of our protocol.
Reporting on race, ethnicity, or other socially relevant groupings	Race, ethnicity, or other social relevant groupings were not considered in this study.
Population characteristics	Human samples were from patients diagnosed with cervical cancer at Shanghai First Maternity and Infant Hospital and Fudan University Shanghai Cancer Center (China). No other population characteristics were considered in the analysis.
Recruitment	Cervical cancer patient samples were obtained at Shanghai First Maternity and Infant Hospital and Fudan University Shanghai Cancer Center after informed consent was obtained. We then selected randomly from the tumor banks. Participants did not receive any compensation. There are no recruitment biases to impact the results of our analyses.
Ethics oversight	These studies using human specimens were approved by the Clinical Research Ethics Committee of Shenzhen University (IACUC, The mechanisms of chromatin remodeling during early stage of DNA damage response, 202400110).

Note that full information on the approval of the study protocol must also be provided in the manuscript.

Field-specific reporting

Please select the one below that is the best fit for your research. If you are not sure, read the appropriate sections before making your selection.

☒ Life sciences ☐ Behavioural & social sciences ☐ Ecological, evolutionary & environmental sciences

For a reference copy of the document with all sections, see nature.com/documents/nr-reporting-summary-flat.pdf

Life sciences study design

All studies must disclose on these points even when the disclosure is negative.

Sample size	In the study, n= at least 3 biological replicates were used for sample size in all cases order to allow statistical analyses. Each biological replicate was defined as an independent culture of cells. Sample sizes were chosen to satisfy statistical power based on previous report (Nat Struct Mol Biol. 2023 .PMID: 37735618). For animal studies, power analyses were determined using a web-based tool (www.biomath.info).
Data exclusions	No data exclusions.
Replication	All the findings were reliably reproduced in multiple biological independent experiments. For all experiments, our data represent at least two independent assays that produce similar results. We also used different assays and readouts to confirm our findings in different way.
Randomization	Cultures and same genotype mice were randomly assigned to either experimental or control groups. For the cell culture experiments, cells were randomly allocated to experimental groups. For all analyses and quantifications, cells were randomly selected. Assigning human samples to experimental groups is not relevant to this study, as the groups are defined by clinical and pathological diagnosis.
Blinding	During sample processing and analysis for MS , qPCR, CUT&tag-seq and ATAC-seq, samples were given a de-identified alphanumeric code. After analysis was completed, samples were unblinded and graphed. The quantification for immunofluorescence assays was performed blindly. In vivo experiments were not blinded during experimentation, although the labels were masked during data analysis.

Reporting for specific materials, systems and methods

We require information from authors about some types of materials, experimental systems and methods used in many studies. Here, indicate whether each material, system or method listed is relevant to your study. If you are not sure if a list item applies to your research, read the appropriate section before selecting a response.

Materials & experimental systems

n/a	Involved in the study
<input type="checkbox"/>	<input checked="" type="checkbox"/> Antibodies
<input type="checkbox"/>	<input checked="" type="checkbox"/> Eukaryotic cell lines
<input checked="" type="checkbox"/>	<input type="checkbox"/> Palaeontology and archaeology
<input type="checkbox"/>	<input checked="" type="checkbox"/> Animals and other organisms
<input checked="" type="checkbox"/>	<input type="checkbox"/> Clinical data
<input checked="" type="checkbox"/>	<input type="checkbox"/> Dual use research of concern
<input checked="" type="checkbox"/>	<input type="checkbox"/> Plants

Methods

n/a	Involved in the study
<input type="checkbox"/>	<input checked="" type="checkbox"/> ChIP-seq
<input type="checkbox"/>	<input checked="" type="checkbox"/> Flow cytometry
<input checked="" type="checkbox"/>	<input type="checkbox"/> MRI-based neuroimaging

Antibodies

Antibodies used

All information of antibodies are described in supplementary table 1. Rabbit monoclonal anti-H1.1 (#ab254394, Abcam, 1:1000), Rabbit polyclonal anti-H1.2 (#ab4086, RRID:AB_2117983, Abcam, 1:1000), Rabbit monoclonal anti-H1.3 (#ab183736, Abcam, 1:1000), Rabbit polyclonal anti-H1.4 (#413285, RRID:AB_2799199, Cell Signaling Technology, 1:1000), Rabbit polyclonal anti-H1.5 (#ab18208, RRID:AB_470263, Abcam, 1:1000), Rabbit polyclonal anti-H3 (#17168-1-AP, RRID:AB_2716755, Proteintech, 1:1000), Mouse monoclonal anti-γH2AX (#80312, RRID:AB_2799949, Cell Signaling Technology, 1:1000), Mouse monoclonal anti-β-actin (#66009-1-Ig, RRID:AB_2687938, Proteintech, 1:1000), Mouse monoclonal anti-FLAG® M2 (#F3165, RRID:AB_259529, Sigma-Aldrich, 1:1000), Rabbit monoclonal anti-pATR (#30632, Cell Signaling Technology, 1:1000), Rabbit polyclonal anti-pNF-κB (#3037, RRID:AB_2341216, Cell Signaling Technology, 1:1000), Rabbit polyclonal anti-53BP1 (#NB100-304, RRID:AB_10003037, Novus Biologicals, 1:1000), Rabbit monoclonal anti-RAD51 (#ab133534, RRID:AB_2722613, Abcam, 1:1000), Rabbit polyclonal anti-CTPS1 (#15914-1-AP, RRID:AB_2086513, Proteintech, 1:1000), Rabbit polyclonal anti-GST (#10000-0-AP, RRID:AB_11042316, Proteintech, 1:1000), Rabbit monoclonal anti-H4 (#13919, RRID:AB_2798345, Cell Signaling Technology, 1:1000), Rabbit monoclonal anti-H2A (#12349, RRID:AB_2687875, Cell Signaling Technology, 1:1000), Rabbit monoclonal anti-H2B (#12364, RRID:AB_2714167, Cell Signaling Technology, 1:1000), Rabbit polyclonal anti-Phospho-(S/T) (#9631, Cell Signaling Technology, RRID:AB_330308, 1:1000), Rabbit polyclonal anti-Acetylated-lysine (#9441, RRID:AB_331805, Cell Signaling Technology, 1:1000), Rabbit polyclonal anti-pan methyl lysine (#ab7315, RRID:AB_305840, Abcam, 1:1000), Rabbit polyclonal anti-PAR (#83732, RRID:AB_2749858, Cell Signaling Technology, 1:1000), Rabbit monoclonal anti-p300 (#863775, RRID:AB_2800077, Cell Signaling Technology, 1:1000), Rabbit monoclonal anti-CBP (#73895, RRID:AB_2616020, Cell Signaling Technology, 1:1000), Rabbit monoclonal anti-hMOF (#ab200660, RRID:AB_2891127, Abcam, 1:1000), Rabbit polyclonal anti-PCAF (#3378, RRID:AB_10679933, Cell Signaling Technology, 1:1000), Rabbit anti-Tip60 (#120585, RRID:AB_2797811, Cell Signaling Technology, 1:1000), Rabbit polyclonal anti-PARP1 (#9542, RRID:AB_2160739, Cell Signaling Technology, 1:1000), Rabbit polyclonal anti-Ki67 (#ab15580, RRID:AB_443209, Abcam, 1:1000), Normal Rabbit IgG (#2729, RRID:AB_1031062, Santa Cruz Biotechnology, 1:1000).

Validation

The validation data for customized antibodies were provided in the manuscript. The validation of commercial antibodies was according to manufacturers' websites or previous reports, listed in supplementary table 1. Rabbit monoclonal anti-H1.1, which is validated in bioRxiv, 2024.2005.2010.593572 (2024). <https://doi.org/10.1101/2024.05.10.593572> Rabbit polyclonal anti-H1.2, which is validated in Mol Cell 77, 475-487 e411 (2020). <https://doi.org/10.1016/j.molcel.2019.10.020> Rabbit monoclonal anti-H1.3, which is validated in Int J Biol Sci 18, 2583-2596 (2022). <https://doi.org/10.7150/ijbs.71519> Rabbit polyclonal anti-H1.4, which is validated in Nat Commun 14, 4991 (2023). <https://doi.org/10.1038/s41467-023-40578-2> Rabbit polyclonal anti-H1.5, which is validated in Cancer Res 82, 2887-2903 (2022). <https://doi.org/10.1158/0008-5472.CAN-22-0717> Rabbit polyclonal anti-H3, which is validated in Nature 587, 673-677 (2020). <https://doi.org/10.1038/s41586-020-2749-z> Mouse monoclonal anti-γH2AX, which is validated in Nat Commun 15, 10596 (2024). <https://doi.org/10.1038/s41467-024-54978-5> Mouse monoclonal anti-β-actin, which is validated in Cell 186, 2208-2218 e2215 (2023). <https://doi.org/10.1016/j.cell.2023.03.032> Mouse monoclonal anti-FLAG® M2, which is validated in Cell Rep 31, 107549 (2020). <https://doi.org/10.1016/j.celrep.2020.107549> Rabbit monoclonal anti-pATR, which is validated in Nature 629, 443-449 (2024). <https://doi.org/10.1038/s41586-024-07350-y> Rabbit polyclonal anti-pNF-κB, which is validated in Nat Commun 14, 1713 (2023). <https://doi.org/10.1038/s41467-023-37450-8> Rabbit polyclonal anti-53BP1, which is validated in Cell Rep 42, 113181 (2023). <https://doi.org/10.1016/j.celrep.2023.113181> Rabbit monoclonal anti-RAD51, which is validated in Nat Commun 15, 3684 (2024). <https://doi.org/10.1038/s41467-024-48149-9> Rabbit polyclonal anti-CTPS1, which is validated in Cancer Res 82, 1013-1024 (2022). <https://doi.org/10.1158/0008-5472.CAN-21-1707> Rabbit polyclonal anti-GST, which is validated in Cell 187, 4272-4288 e4220 (2024). <https://doi.org/10.1016/j.cell.2024.06.024> Rabbit monoclonal anti-H4, which is validated in Nat Commun 15, 9529 (2024). <https://doi.org/10.1038/s41467-024-51847-z> Rabbit monoclonal anti-H2A, which is validated in Nat Commun 15, 9244 (2024). <https://doi.org/10.1038/s41467-024-53639-x> Rabbit monoclonal anti-H2B, which is validated in Nat Commun 14, 4103 (2023). <https://doi.org/10.1038/s41467-023-39735-4> Rabbit polyclonal anti-Phospho-(S/T), which is validated in Nat Commun 15, 1785 (2024). <https://doi.org/10.1038/s41467-024-46166-2> Rabbit polyclonal anti-Acetylated-lysine, which is validated in Sci Adv 10, eadp7423 (2024). <https://doi.org/10.1126/sciadv.adp7423> Rabbit polyclonal anti-pan methyl lysine, which is validated in Cell Discov 7, 37 (2021). <https://doi.org/10.1038/s41421-021-00279-w> Rabbit polyclonal anti-PAR, which is validated in Nat Commun 15, 6641 (2024). <https://doi.org/10.1038/s41467-024-50912-x> Rabbit monoclonal anti-p300, which is validated in Nat Immunol 25, 1580-1592 (2024). <https://doi.org/10.1038/s41590-024-01922-w> Rabbit monoclonal anti-CBP, which is validated in Nat Immunol 25, 1580-1592 (2024). <https://doi.org/10.1038/s41590-024-01922-w> Rabbit monoclonal anti-hMOF, which is validated in Nat Cancer 4, 382-400 (2023). <https://doi.org/10.1038/s43018-023-00522-1> Rabbit polyclonal anti-PCAF, which is validated in Sci Adv 10, eadm9449 (2024). <https://doi.org/10.1126/sciadv.adm9449> Rabbit anti-Tip60, which is validated in Adv Sci (Weinh) 10, e2206584 (2023). <https://doi.org/10.1126/sciadv.adm9449>

doi.org:10.1002/advs.202206584 Rabbit polyclonal anti-PARP1, which is validated in Commun Biol 8, 4 (2025). <https://doi.org:10.1038/s42003-024-07409-6> Rabbit polyclonal anti-Ki67, which is validated in Nat Chem Biol 20, 566-576 (2024). <https://doi.org:10.1038/s41589-023-01466-4> Normal Rabbit IgG, which is validated in Nat Commun 16, 212 (2025). <https://doi.org:10.1038/s41467-024-55768-9>.

Eukaryotic cell lines

Policy information about [cell lines and Sex and Gender in Research](#)

Cell line source(s)	HeLa, HCT116, A549, H1975, HepG2, Hepa1-6, NCI-H1299, HCC1937, MCF7, T47D-KBluc, 786-O, A-498, 5637, T24 and HEK293T cells were obtained from the American Type Culture Collection (Manassas, Virginia, USA). AsiSI-ER-U2OS-AID cells were provided by Dr. Gaëlle Legube (Université Paul Sabatier, Toulouse, France); EJ5-U2OS and DR-U2OS cells were provided by Dr. Xingzhi Xu (Shenzhen University, Shenzhen, China); and U2OS-265 reporter cells were provided by Dr. Roger Greenberg (University of Pennsylvania, USA).
Authentication	Cell lines from ATCC are routinely authenticated by cellular morphology assay. Established stable cell lines were authenticated by PCR and western blot as shown in figures.
Mycoplasma contamination	All cell lines were tested negative mycoplasma contamination.
Commonly misidentified lines (See ICLAC register)	No commonly misidentified cell lines were used.

Animals and other research organisms

Policy information about [studies involving animals](#); [ARRIVE guidelines](#) recommended for reporting animal research, and [Sex and Gender in Research](#)

Laboratory animals	4-week-old BALB/c nude mice were purchased from WuXi AppTec, Guangdong, China. Mice were maintained under SPF conditions in the animal facility of Shenzhen University. The animal room has a controlled temperature (18-23°C), humidity (40-60%), and a 12 light/12 dark cycle.
Wild animals	This study did not involve wild animals.
Reporting on sex	Female
Field-collected samples	This study did not involve samples collected from the field.
Ethics oversight	The use of animals in this study was approved by the Institutional Animal Care and Use Committee (IACUC) of Shenzhen University, China.

Note that full information on the approval of the study protocol must also be provided in the manuscript.

Plants

Seed stocks	NA.
Novel plant genotypes	NA.
Authentication	NA.

ChIP-seq

Data deposition

- ☒ Confirm that both raw and final processed data have been deposited in a public database such as [GEO](#).
- ☒ Confirm that you have deposited or provided access to graph files (e.g. BED files) for the called peaks.

Data access links <i>May remain private before publication.</i>	The data will be accessible before publication. Gene Expression Omnibus under accession number GSE288071.
Files in database submission	ND; ND_4OHT; CT; CT_4OHT; ac; ac_4OHT; aD; aD_4OHT; A; A_4OHT; R_Pi; R_Pi_4OHT; NC; NC_4OHT; SI; SI_4OHT

Genome browser session
(e.g. [UCSC](#))

NA

Methodology

Replicates	CUT&Tag-seq and ATAC-seq samples were prepared as one replicate in each independent experiment.
Sequencing depth	ND, total reads:83638754 ; mapped reads:69445216; reads length: 150bp; paired-end. ND_4OHT, total reads:42723254 ; mapped reads:33936984; reads length: 150bp; paired-end. CT, total reads:42840870 ; mapped reads:34682390; reads length: 150bp; paired-end. CT_4OHT, total reads: 40940896; mapped reads:30074578; reads length: 150bp; paired-end. ac, total reads: 38905586; mapped reads:31263642; reads length: 150bp; paired-end. ac_4OHT, total reads: 37108502; mapped reads:31059092; reads length: 150bp; paired-end. aD, total reads:51580120 ; mapped reads:24507006; reads length: 150bp; paired-end. aD_4OHT, total reads:40205754 ; mapped reads:32056362; reads length: 150bp; paired-end. A, total reads:27629496 ; mapped reads:18820764; reads length: 150bp; paired-end. A_4OHT, total reads:471002 ; mapped reads:465174; reads length: 150bp; paired-end. R_Pi, total reads:1972890 ; mapped reads:10769952; reads length: 150bp; paired-end. R_Pi_4OHT, total reads:53756788 ; mapped reads:33294578; reads length: 150bp; paired-end. NC, total reads:51613294 ; mapped reads:49490948; reads length: 150bp; paired-end. NC_4OHT, total reads:87549828 ; mapped reads:84582728; reads length: 150bp; paired-end. SI, total reads:53402592 ; mapped reads:52786150; reads length: 150bp; paired-end. SI_4OHT, total reads:75508938 ; mapped reads:74137900; reads length: 150bp; paired-end.
Antibodies	Histone modification antibodies were customized; Rabbit polyclonal anti-CTPS1 (#15914-1-AP, RRID:AB_2086513, Proteintech, 1:1000).
Peak calling parameters	NA.
Data quality	Raw data (raw reads) of fastq format were firstly processed using fastp (version 0.19.11, Chen et al., 2018) software. In this step, clean data (clean reads) were obtained by removing reads containing adapter, reads containing poly-N and low quality reads from raw data. At the same time, Q20, Q30 and GC content of the clean data were calculated. All the downstream analyses were based on the clean data with high quality.
Software	Bowtie2 (v 2.5.4) was applied for alignment to the hg38 human genome reference, using the parameters "--very-sensitive --no-mixed --no-discordant." Samtools was used to convert SAM files to BAM format, applying a filter criterion of a minimum mapping quality (MAPQ) score of 10. Duplicate reads were removed using the Picard tool. The bamCoverage function was then used to transform BAM files into BW format, with normalization applied using the parameter "--normalizeUsing BPM." The generation of metagene profiles and heatmaps, which display the signals of each histone modification and open chromatin at double-strand breaks, was accomplished using the computeMatrix and plotHeatmap functions of deepTools (v 3.5.5).

Flow Cytometry

Plots

Confirm that:

- ☒ The axis labels state the marker and fluorochrome used (e.g. CD4-FITC).
- ☒ The axis scales are clearly visible. Include numbers along axes only for bottom left plot of group (a 'group' is an analysis of identical markers).
- ☒ All plots are contour plots with outliers or pseudocolor plots.
- ☒ A numerical value for number of cells or percentage (with statistics) is provided.

Methodology

Sample preparation	For the DR and EJ5 assays, reporter cells were washed with PBS, collected by trypsinization, then assayed for GFP expression by flow cytometry.
Instrument	Becton Dickinson FACSCalibur
Software	Data was collected with FlowJo CE and data was analyzed with FlowJo version 7.6.5 software
Cell population abundance	Cell populations for DR and EJ5 were differentiable by GFP expression above 1000 intensity and quantified with FlowJo.
Gating strategy	For GFP analysis in the DR and EJ5 assay, the GFP threshold for gating was established using the positive control samples and set at 1000 intensity. This gating strategy is shown in the supplementary Information. A negative control sample confirmed this gating strategy, before the exact same gate was applied to all experimental samples.

- ☒ Tick this box to confirm that a figure exemplifying the gating strategy is provided in the Supplementary Information.